Gondwana Research 138 (2025) 192–209

Contents lists available at ScienceDirect

Gondwana Research

journal homepage: www.elsevier.com/locate/gr

# Contrasting physical erosion rates in cratonic catchments: The Ogooué and Mbei rivers, Western Central Africa

V. Regard [a,*], S. Carretier [a], J.-S. Moquet [b], S. Choy [a], P.-H. Blard [c,d], S. Bogning [e], A.P. Mbonda [f], E. Mambela [g], M.C. Paiz [g], M. Séranne [h], J. Charreau [c], D. Rouby [a], J. Bouchez [i], J. Gaillardet [i], J.-J. Braun [a,j,k], Y. Denèle [a]

[a] GET (Université de Toulouse, CNRS, IRD, UPS, CNES), Toulouse, France
[b] Univ. Orléans, CNRS, BRGM, ISTO, UMR 7327, F-45071 Orléans, France
[c] CRPG, CNRS, Université de Lorraine, Nancy, France
[d] Laboratoire de Glaciologie, ULB, Brussels, Belgium
[e] Université de Douala, Cameroon
[f] Centre National de la Recherche Scientifique, Libreville, Gabon
[g] The Nature Conservancy, Libreville, Gabon
[h] Géosciences Montpellier, Université de Montpellier, CNRS, Montpellier, France
[i] IPGP (Université Paris Cité, CNRS, Université La Réunion, IGN), Paris, France
[j] LMI DYCOFAC IRD-University of Yaoundé 1-IRGM, BP 1857, Cameroon
[k] Agence Nationale des Parcs Nationaux, Libreville, Gabon

ARTICLE INFO

Handling Editor: Jan Marten Huizenga

*Keywords:*
Cosmogenic nuclides
Denudation
Chemical weathering
Cratonic areas
Ogooué River

ABSTRACT

We measured the long-term physical denudation of the Ogooué River catchment using $^{10}$Be produced in situ by cosmic rays. These measurements are averaged over 25–200 ka (average 40 ka), depending on the physical denudation rate. The denudation rate of the Ogooué River catchment is slow (38 t/km$^2$/a, 15 m/Ma), slightly higher than in Equatorial West Africa (from Senegal to Angola, 26 t/km$^2$/a, 10 m/Ma). Physical denudation and chemical weathering fall within the same order of magnitude. Thus, although low, there is substantial chemical weathering compared to physical denudation, that likely contributes over 30 % of the total denudation.

Denudation rates are spatially variable (from 10 to 60 t/km$^2$/a) within the large Ogooué River catchment. Over the long term, physical denudation and chemical weathering roughly match, except in the Batéké Plateaux area, because the plateaus are made up of already weathered detrital material and therefore their modern flux of solutes is very low (~9.5 t/km$^2$/a). The spatial distribution is similar to the one described in the work of Moquet et al. (2021) on the basis of solute fluxes, i.e. the southern part of the catchment is denuding twice as fast as the northern part. We show here that the whole picture did not vary much since 100 ka, as shown by both methods which give consistent results. Faster denudation in the southern part of the catchment may be related to more uplift than in the northern part caused by the southern African "superswell".

## 1. Introduction

There is still active debate today on the role of mountains in: (1) global erosion, (2) denudation fluxes, and (3) the production of sediments exported to the ocean (e.g. Willenbring et al., 2013; Larsen et al., 2014; Maffre et al., 2018). Although relatively slow (~120 t/km$^2$/a, equivalent to 45 m/Ma), the denudation of flat continental regions (slope < 200 m/km) results in a significant contribution of sediments to global fluxes given the vast areas involved (Willenbring et al., 2013). Cratonic areas only account for approximately 15 % (according to Şengör et al., 2022) of the catchment-wide denudation rates measured through the cosmogenic isotope $^{10}$Be on detrital sands (from the Octopus database, Codilean et al., 2018). Although a significant body of literature has attempted to identify the controls on denudation rates in tectonically actives areas (e.g. Burbank et al., 1996; Galy and France-Lanord, 2001; Carretier et al., 2013; Godard et al., 2014; Scherler et al., 2017), there are very few similar studies in tectonically inactive regions where mass wasting and faulting are rare.

* Corresponding author at: 14 av. Edouard Belin, 31400 Toulouse, France.
*E-mail address:* Vincent.regard@get.omp.eu (V. Regard).

https://doi.org/10.1016/j.gr.2024.10.013
Received 13 September 2023; Received in revised form 8 October 2024; Accepted 14 October 2024
Available online 8 November 2024

The Ogooué River Basin (ORB) in Gabon, located in Equatorial Africa, (Fig. 1) is particularly suitable for studying the denudation of such tectonically inactive (or low activity) regions since it drains a relatively large area that is representative of the cratonic zones of Equatorial and Tropical West Africa (along the Atlantic coast from Senegal to Angola) and it is underlain by a relatively homogeneous lithology. The catchment is relatively pristine from the perspective of long-term denudation processes and rates, as anthropic pressure has increased only recently.

In the present study, we quantify the catchment-scale denudation rates in nested watersheds across the ORB using *in situ* cosmogenic nuclide measurements on river sands (Fig. 2). However, because of thick regolith layers, cosmogenic nuclide measurements in cratonic areas only record physical denudation, as this method is blind to chemical denudation that occurs deeper than 1 m below the surface (Fig. 3) (Riebe et al., 2003; Granger and Riebe, 2007; Dixon et al., 2009; Hewawasam et al., 2013; Regard et al., 2016). We use chemical denudation estimates for the Ogooué River Basin at the same sites as by Moquet et al. (2021) in order to obtain estimates of the total denudation rates. Our data allow us to quantify the denudation, to estimate the contribution of physical *vs.* chemical processes to the total denudation, and to produce a spatially distributed estimate of these rates within the ORB, providing an opportunity to identify the underlying controls on denudation in this tectonically inactive region.

## 2. Study area

The equatorial Ogooué River Basin (ORB) spans ~ 220,000 km$^2$, from 9 to 14°E and 2.5°N to 3°S (Fig. 1), across the countries of Gabon (85 % of the catchment), Congo (12 %) and Equatorial Guinea and Cameroon (Fig. 1). The river discharge at the mouth is ~ 4,750 m$^3$.s$^{-1}$ (Bogning et al., 2018), corresponding to roughly 10 % of the neighboring Congo River, the largest river in Africa (discharge ~ 41,000 m$^3$.s$^{-1}$; catchment area 3.7 × 10$^6$ km$^2$) (Laraque et al., 2009).

The climate in the Ogooué catchement is tropical *sensu* Köppen-Geiger with one dry season from June to August (Kottek et al., 2006) and with a bimodal precipitation regime with wet periods from March to May and October to December. The average yearly rainfall is approximately 2,000 mm.a$^{-1}$ leading to a runoff of 700 mm.a$^{-1}$ (Bogning et al., 2018; Kittel et al., 2018). The average temperature is constant throughout the year, ~24 °C.

The study area corresponds to 96 % of the Ogooué catchment upstream from the Lambaréné station (206,000 km$^2$, sampling point OG-05, Fig. 1). In addition, we sampled four tributaries of the Mbei River, a tributary of the neighboring Komo River in Northern Gabon which drains terrains that are similar to those underlying the ORB (Fig. 1). The annual discharge of the Mbei River is ~ 60 m$^3$.s$^{-1}$ over an area extending ~ 1,800 km$^2$ (Carré, 1978; Njutapvoui Fokouop, 2017 data for the period 1964–1973 only). The four monitored Mbei tributaries cover an area of less than 500 km$^2$. There, rainfall is ~ 2000 mm.a$^{-1}$ and runoff ~ 600 mm.a$^{-1}$.

Geologically speaking, most of the Ogooué River Basin is developed within plutonic and *meta*-plutonic rocks of the Archean Congo Craton, affected by the Eburnean orogeny in the Paleoproterozoic (Thiéblemont et al., 2009a, 2009b). The lithology of these rocks is predominantly dominated by granites and granitoids, although bands of high-grade metamorphic *meta*-sedimentary rocks are locally observed, such as the

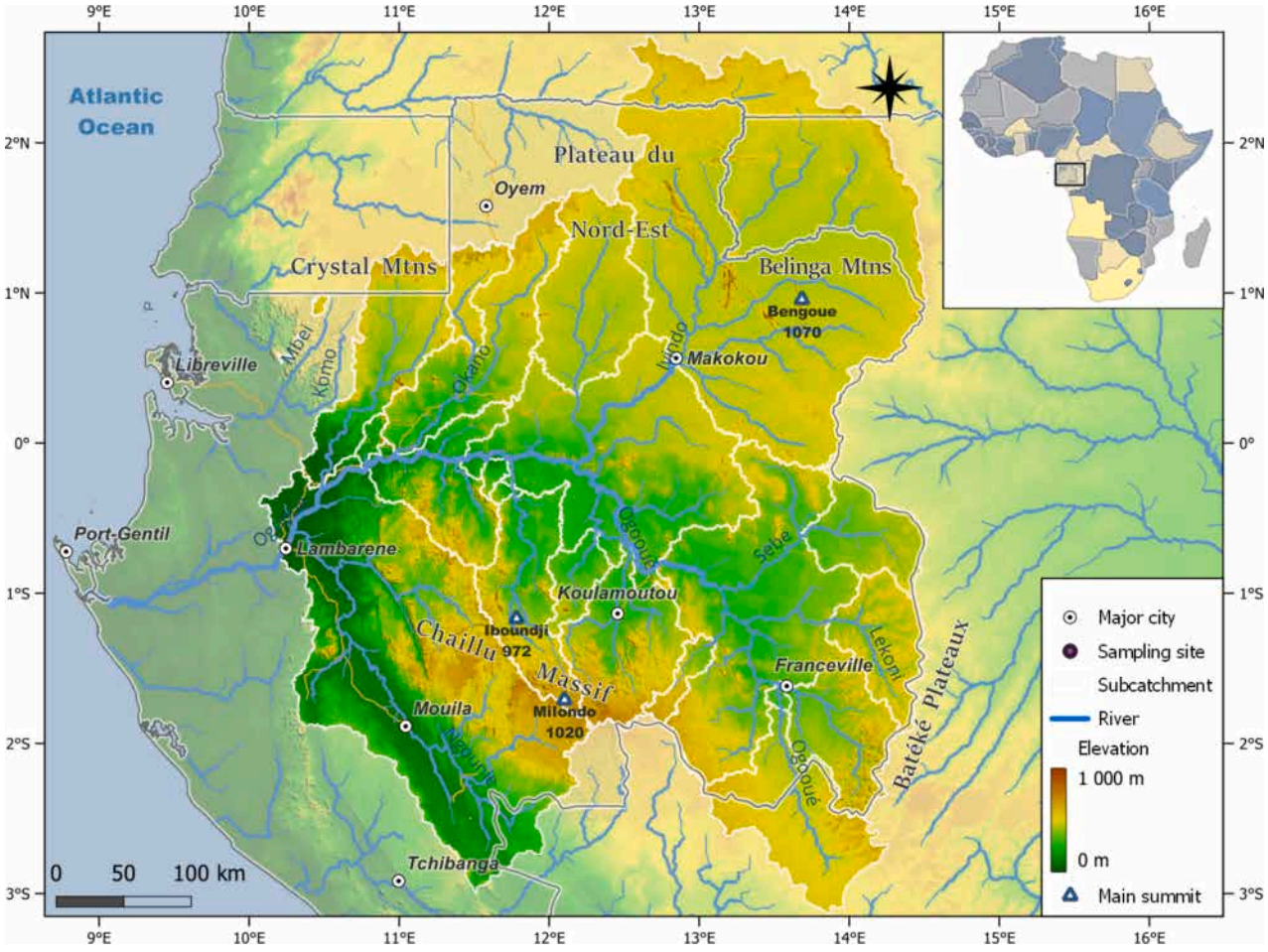


**Fig. 1.** (Inset) map showing the location of the Ogooué river basin (ORB) in Central West Africa. The main map shows the relief, hydrographic network of the Ogooué River, and sampling locations (figure taken from Moquet et al., 2021). The Mbei catchment sampling points are indicated to the north-east.


**Fig. 2.** Photos of the sampling sites along the Ogooué River at Ayem (sampling site #26), upstream (note the people for scale) and downstream. Sand was sampled from the banks at this site.

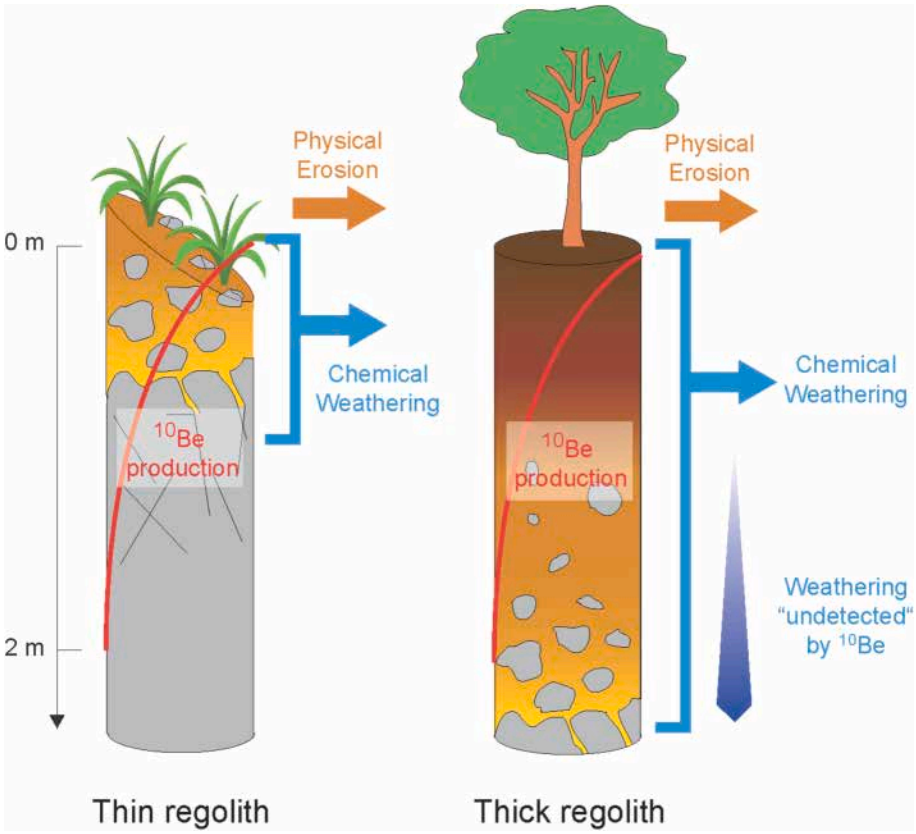


**Fig. 3.** Sketch showing the difference in how chemical weathering is detected by cosmogenic isotopes in the case of a thin (left) vs. thick (right) regolith. Cosmogenic isotope production is high at the surface and decreases rapidly at depth (on a meter scale, as shown in the figure). Thus, the rate of denudation detected by cosmogenic isotopes relates to processes taking place less than around one meter below the surface. If the regolith is thin, then the cosmogenic-derived denudation rate includes both physical and chemical denudation. If the regolith is thick, then cosmogenic isotopes only "see" a part of the chemical denudation, as some of it takes place too deep.

Meso- to Neo-Archean schists and metaconglomerates of the Bélinga Group or the Paleoproterozoic schists of the N'Dolé Group, as well as the Paleoproterozoic micaschists and paragneisses of the Ogoué Complex (Fig. 4). In the southeast, the upstream parts of the basin are located at the Western termination of the Batéké Plateaux, mostly composed of purely quartzitic Cenozoic sandstone (Séranne et al., 2008), and in predominantly detrital sedimentary rocks (pelites, sandstones, and conglomerates) of the Paleoproterozoic Francevillian basins. The sandstone formation of the Batéké Plateaux, discordant on the crystalline basement, is located close to the border with the Congo, where the existence of significant Neogene uplift has been shown, possibly related to mantle swell (Al-Hajri et al., 2009; Guillocheau et al., 2015; Weber et al., 2016). The western and downstream parts of the Ogooué River Basin have mainly developed within the northern termination of the Neoproterozoic orogenic belt of western Congo and in the coastal basin with Phanerozoic lithostratigraphy. In this sector, lithologies are more diverse, with carbonate formations alternating with predominantly fine-grained detrital formations (sandstones and argillites). In summary, the northern tributaries of the Ogooué catchment, as well as the Mbei catchment, exclusively drain Archean cratonic rocks. The southern

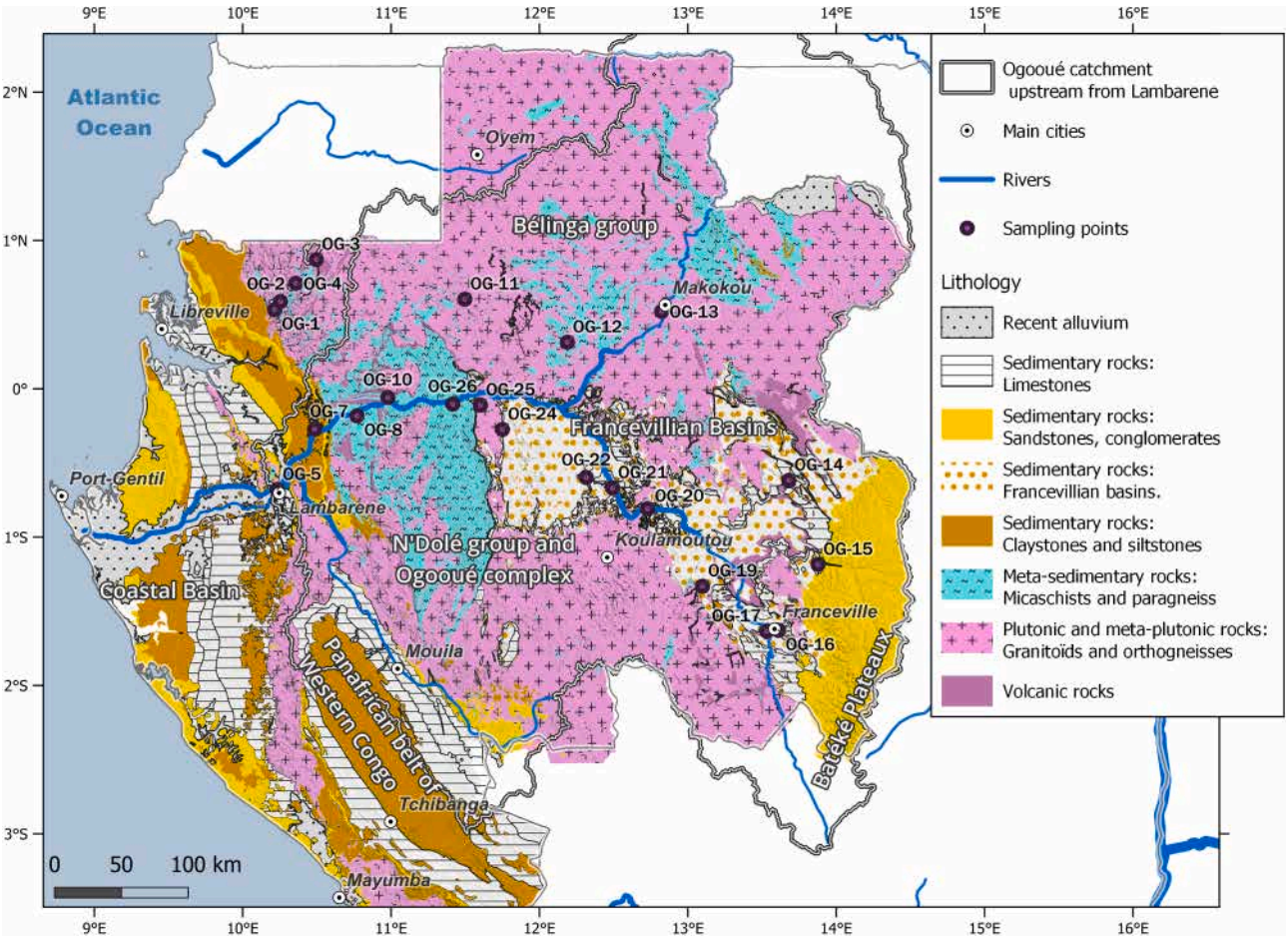


**Fig. 4.** Lithological map of Gabon (Thiéblemont et al., 2009b) with our sampling sites and the Ogooué catchment. The area comprising the metamorphic and plutonic rocks is part of the Congo Craton.

tributaries drain both Archean cratonic rocks and Neoproterozoic volcano-sedimentary rocks. The main Ogooué channel drains Quaternary fluvial sediments in addition to the Mesozoic – Cenozoic basin in its downstream part and the Archean basement in its upstream part Paleoproterozoic Francevilian metasediments in Boumango area) (Thiéblemont et al., 2009a, 2009b) All these lithologies are quartz-rich and are covered by 2- to 3 ka-old, 1–3 m-thick, clayey to sandy laterite-derived aeolian products and regionally known as the "Cover Horizon" (Thiéblemont et al., 2009a).

The elevation of the Ogooué catchment ranges from 20 m.a.s.l. (Lambaréné station) to ~ 1000 m.a.s.l. (Fig. 1); the elevation of the Mbei catchments ranges from 130 to 800 m.a.s.l. The slopes of the Ogooué catchment are low, (~1°), whereas the areas drained by the Mbei tributaries upstream from our sampling sites are steeper, with average slopes up to 7-8° (Moquet et al., 2021).

Following the information provided above, the sampling points and respective catchments are grouped into five areas: (1) the Batéké Plateaux, (2) the northern Ogooué tributaries, (3) the southern Ogooué tributaries, (4) the Ogooué main channel, where fluxes are averaged over catchments from the first three categories, and (5) the Mbei River

**Table 1**
Characteristics of the various areas studied.

| | Batéké Plateaux | Southern tributaries | Northern tributaries | Main Ogooué | Mbei tributaries |
|---|---|---|---|---|---|
| **Lithology (rocks)** | Quartz sandstone | Plutonic, metaplutonic and metasedimentary, volcano-sedimentary | Plutonic, metaplutonic, and metasedimentary rocks | Plutonic, metaplutonic and metasedimentary, volcano-sedimentary, quartz sandstones, limestones | Plutonic, metaplutonic and metasedimentary |
| **Elevation (m)** | 300–800 | 150–1100 | 150–1100 | 150–1100 | 150–750 |
| **Average slope (%)** | 0.8–2 | 1.3–2 | 0.5–3 | 0.5–1.5 | 1–8 |
| **Av. rainfall (mm.a$^{-1}$)** | 2300–2700 | 1900–2600 | ~1900 | 2100–2600 | 1900–2300 |
| **Vegetation** | Extensive agriculture and savanna | Forest | Forest | Forest | Forest |
| **$^{10}$Be denudation rate (m/Ma and t/km$^2$/a)** | 7–22 m/Ma<br>20–60 t/km$^2$/a | 8–20 m/Ma<br>21–51 t/km$^2$/a | 3–8 m/Ma<br>8–22 t/km$^2$/a | 7–18 m/Ma<br>19–48 t/km$^2$/a | 6–23 m/Ma<br>15–60 t/km$^2$/a |
| **Modern TDS flux (** Moquet et al. 2021**)** | 8–12 t/km$^2$/a | 30–53 t/km$^2$/a | 11–22 t/km$^2$/a | 15–20 t/km$^2$/a | 14–18 t/km$^2$/a |

tributaries. The characteristics of these domains are summarized in Table 1.

## 3. Material and methods

### 3.1. Sampling

We collected 22 river sand samples in September 2017: five samples in the Ogooué main channel, 13 samples in the Ogooué's tributaries and four samples in the Mbei River and tributaries (Fig. 4 and Table 2). Three additional samples (labelled BTK) were collected previously during another campaign in January and February 2008: BTK08-22 on the main Ogooué River upstream (just upstream of sample OG-17 from the 2017 campaign); BTK08-5 from the Léconi River, a tributary of the Ogooué, collected at a location very close to sample OG-15 from 2017; and BTK08-20 from the Socle River, a southern tributary of the Ogooué, quite close to the 2017 OG-19 sample on the Leyou, where the river only drains Archean plutonic rocks. Approximately 1 kg of sand was collected at each sampling point from recently deposited riverbanks. The sampled sands consist almost entirely of quartz, as commonly observed for lowland tropical rivers, making it easy to carry out the chemical treatment described below.

### 3.2. Measurement of the in-situ $^{10}$Be concentrations

All samples were processed for *in situ* beryllium-10 ($^{10}$Be) at GET (Géosciences Environnement Toulouse), with the exception of samples BTK08-5, BTK08-20 and BTK08-22 which were processed at CRPG (Centre de Recherches Pétrographiques et Géochimiques, Nancy) for both $^{10}$Be and aluminium-26 ($^{26}$Al), following the procedure described in Puchol et al. (2017).

The samples were first sieved to extract the 500–1000 μm size fraction, which then underwent a series of acid attacks with a mixture of concentrated hydrochloric (HCl) and hexafluorosilisic ($H_2SiF_6$) acids to remove all non-quartz minerals. Meteoric $^{10}$Be was then removed by three partial leaching steps with concentrated hydrofluoric acid (HF). The leached quartz was dissolved with concentrated hydrofluoric acid (HF) after adding a $^{9}$Be carrier solution (500 μL of a [$^{9}$Be] = 1000 μg/g solution for the GET batch, and 100 mg of a [$^{9}$Be] = 3066 μg/g solution for the CRPG batch). The resulting solutions were evaporated until dryness and the samples were recovered with hydrochloric acid. Dissolved species were then precipitated with concentrated ammonia before processing through an anion exchange column to remove the iron, and a cation exchange column to discard the boron and recover Be (as well as Al for two samples processed at CRPG). After elution, Be was precipitated as $Be(OH)_2$ by adding concentrated ammonia at pH = 8 and oxidized to BeO. After preparing the target by mixing niobium powder with the BeO oxide, the $^{10}$Be/$^{9}$Be ratios were measured by Accelerator Mass Spectrometry (AMS) at the French National AMS Facility ASTER of CEREGE in Aix-en-Provence (Arnold et al., 2010). In the case of the GET batch, the measured $^{10}$Be/$^{9}$Be ratios were calibrated against an in-house standard STD-11 with an assigned value of (1.191 ± 0.013) × $10^{-11}$ (Braucher et al., 2015), while the CRPG batch was calibrated against the SRM 4325 NIST reference material, using a $^{10}$Be/$^{9}$Be ratio of (2.79 ± 0.03) x $10^{-11}$ (Nishiizumi et al., 2007). Both are similar to the KNSTD07 calibration (Balco et al., 2008; Nishiizumi et al., 2007). The analytical 1σ uncertainties include uncertainties in the AMS counting statistics, the uncertainty in the standard $^{10}$Be/$^{9}$Be ratio, an external AMS error of 0.5 % (Arnold et al., 2010), and a chemical blank correction (that yielded $^{10}$Be/$^{9}$Be ratios of (9.9 ± 0.6) × $10^{-15}$, (9.8 ± 0.6) × $10^{-15}$, and (2.1 ± 1.0) × $10^{-15}$ for the first GET, second GET, and CRPG batches, respectively; Table 2). A $^{10}$Be half-life of 1.387 ± 0.01 Ma was used (Chmeleff et al., 2010; Korschinek et al., 2010).

For the specific case of the samples processed for the $^{26}$Al measurements, the $^{27}$Al concentrations were measured from small aliquots of the dissolved samples, after evaporation and substitution of fluorides by $HNO_3$. This measurement was done by inductively coupled plasma optical emission spectrometry (ICP-OES) at the Service National d'Analyse des Roches et Minéraux (SARM, CRPG, Vandoeuvre, France). The $^{26}$Al/$^{27}$Al ratios measured at ASTER were normalized to the ASTER in-house standard SM-Al-11, with a $^{26}$Al/$^{27}$Al value of (7.40 ± 0.06) × $10^{-12}$. The analytical $^{26}$Al/$^{27}$Al blank ratio was (3 ± 3) × $10^{-15}$.

### 3.3. Calculation of the $^{10}$Be-derived, catchment-wide denudation rates

The catchment-scale denudation rates were calculated neglecting the radioactive decay, as per Lupker et al. (2012):

$$\overline{\varepsilon} = \frac{P_n\mu_n + P_{sm}\mu_{sm} + P_{fm}\mu_{fm}}{\rho[CN]}$$

Where $\overline{\varepsilon}$ the mean denudation rate in cm/a; ρ is the rock density (= 2.7 g/cm$^3$); [CN] is the cosmogenic nuclide concentration (at/g); $P_n$, $P_{sm}$ and $P_{fm}$ (at/g/a) are the catchment average cosmogenic nuclide production rates by neutrons, slow muons, and fast muons, respectively, and $\mu_n$, $\mu_{sm}$ and $\mu_{fm}$ (g/cm$^2$) are the attenuations for neutrons, slow muons, and fast muons, respectively. The average $^{10}$Be production rates for each cosmogenic production pathway were calculated using a cell-by-cell approach and the Basinga GIS toolbox (Charreau et al., 2019). In this toolbox, the mean sea surface level high latitude (SLHL) production rate is 4.18 at/g (Martin et al., 2017) and includes 98.86 %, 0.27 % and 0.87 % atoms produced by neutrons, slow muons and fast muons, respectively (Martin et al., 2017 after; Braucher et al., 2011). From this SLHL value, the $^{10}$Be production rates were calculated for each pixel (90 m resolution, from a SRTM 3 arc-seconds DEM) of the catchment area overlying a quartz-hosting lithology, scaled for latitude (neutrons only) and elevation (neutrons and muons) using the scaling models of Stone (2000) and the ERA-40 atmosphere atlas (Uppala et al., 2005). Following the recommendation from DiBiase (2018), no topographic shielding factor was applied. All pixel values were then averaged within each catchment to determine $P_n$, $P_{sm}$, and $P_{fm}$. The denudation rate uncertainty was calculated by propagating the analytical uncertainty on [CN] and a 15 % uncertainty on the production rates. To test for the possibility of a bias associated with the abundance of quartz, variable quartz percentages were assigned to the different lithologies present in this catchment. The $^{10}$Be production rates are weighted by these quartz percentages according to Carretier et al. (2015). The resulting denudation rates are within 1.5 % equal to those calculated with a constant quartz abundance, reported in Table 3. We estimate that for denudation rates of between 8 and 30 m/Ma, neglecting radioactive decay only results in an overestimate between 15 and 5 % of the denudation rate, which remains within the uncertainty associated with the assumed uncertainty of 15 % for the production rate.

The time over which cosmogenic nuclides are averaging catchment-wide erosion rates is called the integration time (τ). It corresponds to the time required to remove one attenuation length (L = $\mu_n/\rho$ [cm]) from the Earth surface. For this calculation, only spallation by neutrons is considered: $\tau = L/\overline{\varepsilon}$. It should be noted that this method captures all the denudation processes that take place close to the surface (max depth ~ L), so we use the term denudation. To calculate the total denudation, i.e. taking the deeper weathering processes into account, it is necessary to use independent measurements of weathering rates or to make necessary assumptions, which will be the subject of section 4.3.

It should be noted that the "Cover Horizon" has probably disturbed the steady-state condition necessary for the use of cosmogenic nuclides to measure denudation rates. However, as this perturbation is very recent, we can assume, following Ferrier and Kirchner (2008), that the denudation rate evaluation is robust to such a small deviation from the steady state. This is further illustrated by the fact that the integration time (τ) is much larger than the age of the cover horizon (2–3 ka).

**Table 2**
$^{10}$Be and $^{26}$Al analytical data. The uncertainties are 1σ. See text for methods and calibrations.

| Sample name | Sample code | Location | River | Latitude (°N) | Longitude (°E) | Elevation (m asl) | Domain | Dissolved Quartz (g) | $^{9}$Be added through carrier ($10^{15}$ at) | Uncertainty | Measured $^{10}$Be/ $^{9}$Be (x $10^{15}$) | Uncertainty (%) | $^{10}$Be (at/ g) | Uncertainty | $^{27}$Al content ($10^{15}$ at) | Uncertainty | Measured $^{26}$Al/ $^{27}$Al (x $10^{-15}$) | Uncertainty (%) | $^{26}$Al (at/ g) | Uncertainty |
|---|---|---|---|---|---|---|---|---|---|---|---|---|---|---|---|---|---|---|---|---|
| **First series of samples†** | | | | | | | | | | | | | | | | | | | | |
| **OG-01** | **01** | | | 0.5332 | 10.2148 | 139 | Mbei | 20.96 | 34 194 | 102 | 58 | 4.34 % | 94 690 | 3 374 | | | | | | |
| **OG-02** | **02** | Akelayong | Mbei | 0.5874 | 10.2541 | 160 | Mbei | 20.85 | 34 167 | 102 | 218 | 2.77 % | 357 636 | 9 126 | | | | | | |
| **OG-03** | **03** | Akoga | Mwenge | 0.8709 | 10.4961 | 534 | Mbei | 20.79 | 34 067 | 101 | 223 | 2.62 % | 365 831 | 8 814 | | | | | | |
| **OG-04** | **04** | Assok | Binguili | 0.7110 | 10.3570 | 526 | Mbei | 19.46 | 34 180 | 102 | 163 | 3.19 % | 287 148 | 8 320 | | | | | | |
| **OG-05** | **05** | Lambaréné | Ogooué | −0.6804 | 10.2313 | 2 | Ogooué main channel | 20.91 | 33 993 | 101 | 92 | 3.86 % | 150 272 | 5 031 | | | | | | |
| **OG-07** | **07** | Abanga | Abanga | −0.2726 | 10.4847 | 16 | Northern tributaries | 20.47 | 34 046 | 101 | 160 | 3.62 % | 266 179 | 8 833 | | | | | | |
| **OG-08** | **08** | Ndjolé | Ogooué | −0.1827 | 10.7701 | 16 | Ogooué main channel | 19.70 | 34 267 | 102 | 85 | 4.27 % | 148 466 | 5 519 | | | | | | |
| **OG-10** | **10** | Alembé | Ogooué | −0.0591 | 10.9782 | 46 | Northern tributaries | 20.18 | 34 040 | 101 | 204 | 3.57 % | 343 595 | 11 444 | | | | | | |
| **OG-11** | **11** | Mindzi | Lara | 0.6034 | 11.4966 | 313 | Northern tributaries | 20.22 | 34 160 | 102 | 278 | 3.38 % | 470 474 | 15 072 | | | | | | |
| **OG-12** | **12** | Ovan | Mvoung | 0.3136 | 12.1879 | 404 | Northern tributaries | 20.12 | 34 046 | 101 | 260 | 2.56 % | 439 423 | 10 469 | | | | | | |
| **OG-13** | **13** | Loaloa | Ivindo | 0.5215 | 12.8245 | 462 | Northern tributaries | 20.04 | 34 153 | 102 | 442 | 2.28 % | 752 413 | 16 405 | | | | | | |
| **OG-14** | **14** | Okandja | Sébé | −0.6176 | 13.6812 | 295 | Batéké Plateaux | 12.87 | 33 933 | 101 | 61 | 4.07 % | 161 295 | 5 384 | | | | | | |
| **OG-15** | **15** | Akieni | Léconi | −1.1852 | 13.8773 | 387 | Batéké Plateaux | 22.22 | 34 060 | 101 | 217 | 2.79 % | 332 742 | 8 575 | | | | | | |
| **OG-16** | **16** | Franceville | Passa | −1.6294 | 13.6103 | 287 | Batéké Plateaux | 22.66 | 33 384 | 99 | 69 | 4.20 % | 101 983 | 3 604 | | | | | | |
| **Chemical blank** | | | | | | | | 33 993 | 101 | 9.92 | 5.58 % | | | | | | | | | |
| **Second series of samples†** | | | | | | | | | | | | | | | | | | | | |
| **OG17** | **17** | Franceville | Ogooué | −1.6355 | 13.5314 | 285 | Ogooué main channel | 21.26 | 34 060 | 101 | 209 | 3.39 % | 334 443 | 10 475 | | | | | | |
| **OG19** | **19** | Ndoubi | Leyou | −1.3313 | 13.0989 | 293 | Southern tributaries | 23.67 | 34 127 | 102 | 91 | 4.08 % | 131 902 | 4 614 | | | | | | |
| **OG20** | **20** | Lastourville | Ogooué | −0.8096 | 12.7285 | 228 | Ogooué main channel | 22.38 | 33 873 | 101 | 85 | 3.99 % | 127 982 | 4 312 | | | | | | |
| **OG21** | **21** | Lolo | Lolo | −0.6685 | 12.4929 | 213 | Southern tributaries | 19.80 | 33 919 | 101 | 71 | 4.24 % | 121 210 | 4 256 | | | | | | |
| **OG22** | **22** | Wagny | Ouagna | −0.5988 | 12.3150 | 201 | Southern tributaries | 24.14 | 33 411 | 99 | 150 | 3.70 % | 207 510 | 6 925 | | | | | | |
| **OG24** | **24** | Parc Lopé | Offoué | −0.2744 | 11.7502 | 145 | Southern tributaries | 21.35 | 34 107 | 101 | 100 | 4.27 % | 160 380 | 5 981 | | | | | | |
| **OG25** | **25** | Lopé | Offoué | −0.1102 | 11.6019 | 118 | Southern tributaries | 19.90 | 34 127 | 102 | 146 | 3.49 % | 251 038 | 7 836 | | | | | | |
| **OG26** | **26** | Ayem | Ogooué | −0.1037 | 11.4153 | 88 | Ogooué main channel | 22.39 | 34 046 | 101 | 83 | 3.96 % | 126 564 | 4 222 | | | | | | |
| **Chemical blank** | | | | | | | | 33 859 | 101 | 9.75 | 6.39 % | | | | | | | | | |

(*continued on next page*)

**Table 2** (*continued*)

| Sample name | Sample code | Location | River | Latitude (°N) | Longitude (°E) | Elevation (m asl) | Domain | Dissolved Quartz (g) | $^{9}$Be added through carrier ($10^{15}$ at) | Uncertainty | Measured $^{10}$Be/ $^{9}$Be (x $10^{15}$) | Uncertainty (%) | $^{10}$Be (at/g) | Uncertainty | $^{27}$Al content ($10^{15}$ at) | Uncertainty | Measured $^{26}$Al/ $^{27}$Al (x $10^{-15}$) | Uncertainty (%) | $^{26}$Al (at/g) | Uncertainty |
|---|---|---|---|---|---|---|---|---|---|---|---|---|---|---|---|---|---|---|---|---|
| **Third series of samples‡** | | | | | | | | | | | | | | | | | | | | |
| **BTK08-5** | **08–5** | Akiéni | Léconi | −1.1801 | 13.8917 | 440 | Batéké Plateaux | 25.98 | 20 425 | | 130 | 3.77 % | 206 160 | 7 766 | 33 551 | 554 | 670 | 4.78 % | 864 754 | 41 310 |
| **BTK08-20** | **08–20** | Bakoumba | Socle | −1.8633 | 13.0138 | 537 | Southern tributaries | 18.93 | 20 685 | | 146 | 3.09 % | 126 577 | 3 907 | | | | | | |
| **BTK08-22** | **08–22** | Poubara | Ogooué | −1.7623 | 13.5450 | 395 | Ogooué main channel | 30.41 | 20 359 | | 94 | 3.09 % | 321 498 | 9 948 | 25 955 | 636 | 1 257 | 3.07 % | 1 722 966 | 52 842 |
| **Chemical blank** | | | | | | | | | | 2.1 | 47.62 % | | | | | 3 | 100 % | | | |

† prepared at GET, ‡ prepared at CRPG.

### 3.4. Chemical denudation rates

Our sampling sites in the ORB are constrained for total dissolved solids (TDS) by the study of Moquet et al. (2021), which enables the estimation of the chemical denudation rates when used in combination with long-term water discharge estimates. However, because the river hydrochemistry at the sampling sites has only been measured once, the relevance of the calculated solute fluxes might be questioned in terms of long-term denudation, due to variable solute concentrations over a one year period. Moquet et al. (2021) noted that in other West African rivers such as the Nyong (Viers et al., 2000), Niger (Picouet et al., 2002) and Congo (Laraque et al., 2009), the TDS concentration varies only slightly with discharge over the year, meaning that solute fluxes in these rivers are mainly controlled by discharge variability, thereby lending confidence to the solute flux estimates based on the hydrochemistry measured during a single sampling campaign. The propagation of various sources of uncertainties, which include the single point sampling strategy, has been estimated and described by Moquet et al. (2021, section 3.7 "Uncertainty calculation"). Therefore, the uncertainties associated with the chemical weathering flux used in the present paper includes this source of uncertainty. The long-term discharge (multi-year) at the sampling sites was estimated through a statistical approach based on a regional polynomial regression between specific discharge ($Q_{spe}$) and rainfall ($P$) (see Moquet et al., 2021 for details). As outlined by Moquet et al. (2021), we can reasonably consider that the studied rivers tend to exhibit a so-called "chemostatic behavior" which indicates that, despite the fact that some variability in the solute concentration exists, a single sampling point in space can be used to produce reasonable, first-order estimates of catchment-scale weathering rates.

In the ORB, most of the river solute flux is derived from silicate chemical weathering; < 15 % is derived from atmospheric inputs (Moquet et al., 2021). Low cationic weathering rates are observed for the Batéké Plateaux ($TZ^{+}_{sil}$ ~0.5 t/km$^2$/a, where $TZ^{+}_{sil}$ represents the chemical weathering rate expressed as the release rate of the sum of cations by silicate chemical weathering). Higher weathering rates are typical of the southern catchments ($TZ^{+}_{sil}$ ~3.4 t/km$^2$/a), and intermediate rates ($TZ_{sil}$ between 1.7 and 2.5 t/km$^2$/a), similar to those observed for the Ogooué River at its mouth, characterize the northern catchments and the Mbei tributaries.

## 4. Results

The $^{10}$Be concentrations of the Ogooué sediments show an average catchment denudation rate of approximately 15 m/Ma (~40 t/km$^2$/a, Fig. 5). We obtained these values for the two most downstream samples (OG-5 and OG-8), which integrate most of the catchment area (~200,000 km$^2$). Following Moquet et al. (2021), we divide the samples into five groups following geomorphological and lithological units (Table 2, Fig. 1): the Mbei tributaries (outside of the Ogooué catchment itself), the northern Ogooué tributaries, the Batéké Plateaux tributaries, the southern Ogooué tributaries, and the Ogooué River main channel.

The two most downstream samples (OG-5 and OG-8) integrate most of the catchment area (~200,000 km$^2$) and provide the average catchment denudation rate. Along the Ogooué main channel, upstream from the lowermost sample (samples OG-5, OG-8, OG-26, OG-20, OG-17 and BTK08-22 in the upstream direction), the evolution of $^{10}$Be concentration is not monotonous, with lower concentrations for samples OG-26 and OG-20; this results in higher denudation rates of ~ 17 m/Ma, 47 t/km$^2$/a. In comparison, the most upstream Ogooué mainstream sampling site (samples OG-17 and BTK08-22,) displays a higher $^{10}$Be concentration, implying a lower denudation rate of 7 m/Ma or 18 t/km$^2$/ a (Table 3 and Figs. 5 and 6). The rivers draining the Batéké Plateaux represent the main contributors to the Ogooué between sampling points OG-17 and OG-20.

The denudation rates in the Batéké Plateaux area (samples OG-14, OG-15, OG-16, and BTK08-5) are variable, ranging from 7 to 22 m/

**Table 3**

| Sample name | Production | Difference Quartz | Denudation | Uncertainty | Denudation | Uncertainty | Integration time |
|---|---|---|---|---|---|---|---|
| | at/g/a | % | m/Ma | | t/km$^2$/a | | ka |
| **OG-01** | 3.10 | 1.50 | 23.0 | 1.9 | 62.1 | 5.0 | 26 |
| **OG-02** | 2.92 | 0 | 5.8 | 0.5 | 15.6 | 1.2 | 104 |
| **OG-03** | 3.54 | −0.19 | 6.7 | 0.5 | 18.1 | 1.3 | 89 |
| **OG-04** | 3.57 | 0.04 | 8.7 | 0.7 | 23.4 | 1.7 | 69 |
| **OG-05** | 3.11 | 0.05 | 14.6 | 1.2 | 39.3 | 3.1 | 41 |
| **OG-07** | 3.14 | −0.15 | 8.3 | 0.7 | 22.3 | 1.7 | 73 |
| **OG-08** | 3.16 | 0.07 | 15.0 | 1.2 | 40.4 | 3.2 | 40 |
| **OG-10** | 3.12 | −0.04 | 6.4 | 0.5 | 17.2 | 1.3 | 94 |
| **OG-11** | 3.30 | 0 | 4.9 | 0.4 | 13.2 | 1.0 | 122 |
| **OG-12** | 3.23 | 0.01 | 5.1 | 0.4 | 13.9 | 1.0 | 117 |
| **OG-13** | 3.30 | 0.06 | 3.1 | 0.2 | 8.3 | 0.6 | 196 |
| **OG-14** | 3.07 | 0 | 13.4 | 1.1 | 36.3 | 2.9 | 45 |
| **OG-15** | 3.27 | 0 | 6.9 | 0.5 | 18.5 | 1.4 | 87 |
| **OG-16** | 3.23 | 0 | 21.8 | 1.8 | 58.9 | 4.7 | 28 |
| **OG-17** | 3.37 | −0.10 | 7.0 | 0.5 | 18.9 | 1.4 | 86 |
| **OG-19** | 3.44 | −0.15 | 18.1 | 1.4 | 48.9 | 3.7 | 33 |
| **OG-20** | 3.16 | 0.09 | 17.3 | 1.4 | 46.8 | 3.6 | 35 |
| **OG-21** | 3.27 | 0.04 | 18.8 | 1.5 | 50.8 | 3.9 | 32 |
| **OG-22** | 3.27 | 0.04 | 11.0 | 0.9 | 29.7 | 2.3 | 55 |
| **OG-24** | 3.17 | 0.02 | 13.8 | 1.1 | 37.4 | 2.9 | 43 |
| **OG-25** | 2.79 | 0 | 7.9 | 0.6 | 21.3 | 1.7 | 76 |
| **OG-26** | 3.19 | 0.08 | 17.6 | 1.4 | 47.6 | 3.7 | 34 |
| **BTK08-5** | 3.27 | 0 | 11.1 | 0.9 | 29.9 | 2.3 | 54 |
| **BTK08-20** | 3.63 | 0 | 19.8 | 1.5 | 53.3 | 3.8 | 30 |
| **BTK08-22** | 3.37 | 0 | 7.3 | 0.6 | 19.8 | 1.5 | 82 |

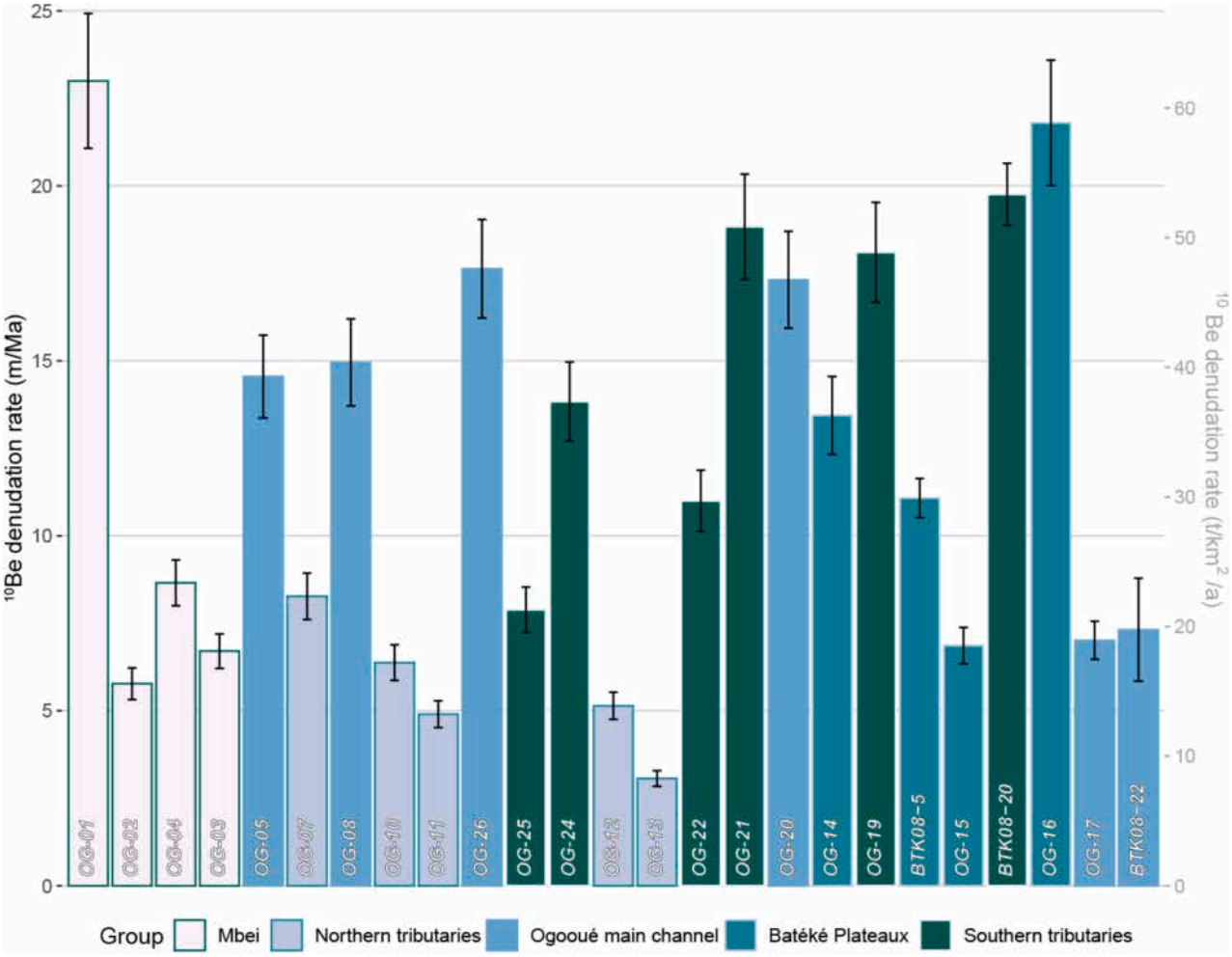


**Fig. 5.** The $^{10}$Be-derived denudation rates, ordered from downstream to upstream along the Ogooué main channel. The Mbei rivers (samples# 1 to 4) do not drain to the Ogooué River.

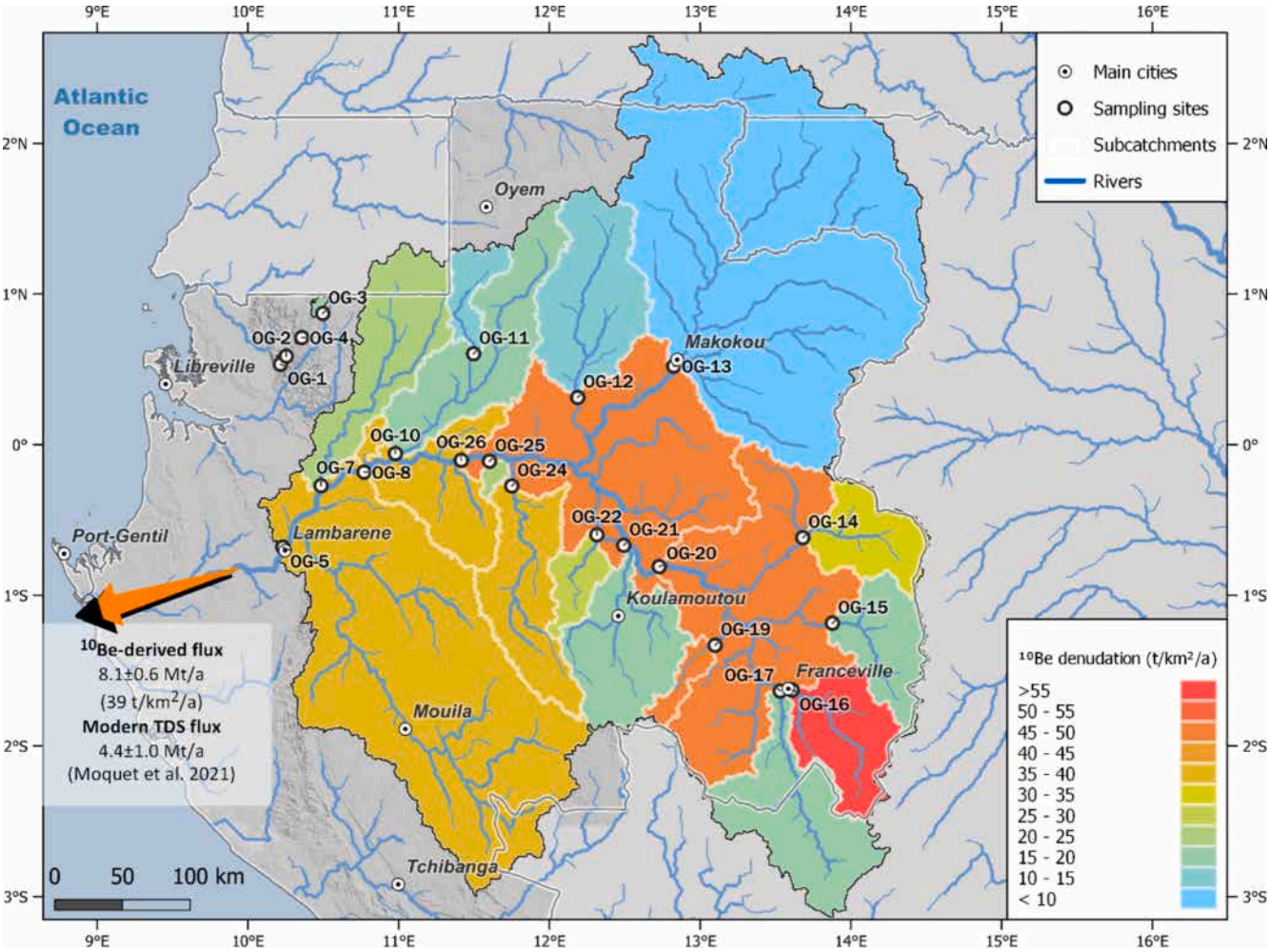


**Fig. 6.** Colored scale map of the $^{10}$Be-derived catchment-scale denudation rates for the ORB. The sampling points that define the outlets of the catchment areas are shown as black open circles. The modern TDS flux has been evaluated by Moquet et al. (2021).

Ma (18 to 57 t/km$^2$/a). The denudation rates of the northern tributaries (3–7 m/Ma or 8–19 t/km$^2$/a) are roughly one or two times lower than those of the southern tributaries (8–20 m/Ma or 21–53 t/km$^2$/a). The trend in the catchment-scale denudation rate observed along the course of the Ogooué River mainstream (Fig. 5) most likely results from the contribution of these tributaries.

The position of two samples draining the Batéké Plateaux (BTK08-5 and BTK08-22) in a "banana plot" ($^{26}$Al/$^{10}$Be *vs.* $^{10}$Be; Figure S1) indicates that these samples are partly made up of recycled material. However, the proximity of the data to the "surface banana" (in black on Figure S1) suggests that the contribution of this recycled material is low, resulting in an underestimate of the $^{10}$Be-derived denudation rate by 25 % at most.

The spatial distribution of the denudation rates in the Ogooué catchment can be refined using a "nested catchment approach", where the difference in sediment flux (calculated as the erosion rate x the contributing area) between two stations along the same river provides an estimate of the sediment flux and the erosion rates of the area contributing to the river between these two stations. Despite significant uncertainties (see Supplementary Material Figure S2), these estimates: 1) result in values similar to those stemming from direct $^{10}$Be measurements for samples OG-5 and OG-10 (Fig. 5), and 2) suggest an erosion that is faster than 80 t/km$^2$/a for the two nested catchments (OG-20 and OG-26). However, because of the significant uncertainties associated with these estimates, we do not include these numbers in the analysis presented in section 4.2.

We evaluated the interannual variability in the $^{10}$Be-derived erosion rate using pairs of samples collected at the same location in 2008 and in 2017. Samples OG-17 and BTK08-22, from the upstream part of the main Ogooué channel, result in similar erosion rates within uncertainty, whereas the $^{10}$Be-derived erosion rate from samples OG-15 and BTK08-05, from the Batéké Plateaux, differ by 25 %. This difference could come from the variable contribution from the sub-catchments to the sand collected at the sampling sites, and indicates that in addition to analytical uncertainties, long-term estimates of the erosion rates of large, lithologically-mixed catchments of the ORB are affected by other sources of uncertainties, that we estimate to be on the order of 25 %.

### 4.1. $^{10}$Be denudation rates vs. Catchment physical properties

Table 4 summarizes the catchment-scale physical and geomorphological parameters and denudation flux from this work and the chemical denudation rates from Moquet et al. (2021). As commonly observed, the denudation rates increase with the slope, even for low slopes such as those prevailing in the ORB (Fig. 7a). The two points that deviate from this relationship are two catchments of the Mbei tributaries, which are most likely too small to be accurately represented by the DEM. The denudation rates do not vary significantly with rainfall (which is relatively invariant across the study area; Fig. 7b), catchment elevation (Fig. 7c), or river discharge (Fig. 7d), as also emphasized by the correlation matrix (Fig. 8). In addition, Fig. 7e shows that the $^{10}$Be integration time decreases with the catchment size, except for the northern

**Table 4**
Modern dissolved fluxes († refers to data from Moquet et al., 2021) *vs.* millennial fluxes. The fluxes are organized by group; the second part of the table indicates group averages and the third one (lowermost) shows the fluxes evaluated by the nested catchment method (see the text and Supplementary Material S2). The catchment properties, Total Dissolved Solids (TDS), results from the $^{10}$Be concentrations (denudation rate and fluxes), and integration time are displayed from left to right).

| Group | Sample number | Basin area† | Basin average slope† | Basin average elevation† | River annual mean discharge† | Basin average rainfall† | Specific discharge (runoff)† | Modern TDS flux† | Modern TDS flux† | Millenial area-normalized fluxes ($^{10}$Be) | | | | |
|---|---|---|---|---|---|---|---|---|---|---|---|---|---|---|
| | | | | | | | | | | Denudation | Denudation uncertainty | Flux | Flux uncertainty | Integration time |
| | | km$^2$ | % | m.a.s.l. | m$^3$/s | mm a$^1$ | mm a$^{-1}$ | $10^3$ t a$^{-1}$ | t km$^{-2}$ a$^{-1}$ | t km$^{-2}$ a$^{-1}$ | t km$^{-2}$ a$^{-1}$ | $10^3$ t a$^{-1}$ | $10^3$ t a$^{-1}$ | $10^3$ a |
| | 1 | 13 | 7.9 | 448 | 0.29 | 2244 | 692 | 0.24 | 18 | 62.1 | 5.0 | 0.8 | 0.1 | 26 |
| Mbei tributaries | 2 | 5 | 7.5 | 387 | 0.11 | 2244 | 692 | 0.09 | 17.2 | 15.6 | 1.2 | 0.1 | 0.0 | 104 |
| | 3 | 135 | 1 | 639 | 2.6 | 1957 | 604 | 1.86 | 13.8 | 18.1 | 1.3 | 2.4 | 0.2 | 89 |
| | 4 | 13 | 0.8 | 613 | 0.29 | 2244 | 692 | 0.21 | 15.8 | 23.4 | 1.7 | 0.3 | 0.0 | 69 |
| | 18 & 08-22 | 8778 | 0.7 | 582 | 229 | 2663 | 821 | 158 | 18 | 19.8 | 1.5 | 173.4 | 12.7 | 82 |
| | 17 | 14,944 | 1 | 555 | 390 | 2672 | 824 | 276 | 18.5 | 18.9 | 1.4 | 282.9 | 21.2 | 86 |
| Ogooué main channel | 20 | 45,823 | 1.1 | 493 | 1126 | 2512 | 775 | 705 | 15.4 | 46.8 | 3.6 | 2142.5 | 165.2 | 35 |
| | 26 | 142,373 | 0.9 | 502 | 3044 | 2186 | 674 | 2764 | 19.4 | 47.6 | 3.7 | 6778.3 | 520.8 | 34 |
| | 8 | 160,312 | 1 | 497 | 3378 | 2155 | 664 | 3007 | 18.8 | 40.4 | 3.2 | 6473.2 | 517.7 | 40 |
| | 5 & 6 | 205,585 | 1.2 | 467 | **4341*** | 2159 | 666 | 4071 | 19.8 | 39.3 | 3.1 | 8077.5 | 632.9 | 41 |
| | 7 | 8265 | 1.3 | 448 | 155 | 1915 | 590 | 177.8 | 21.5 | 22.3 | 1.7 | 184.5 | 14.2 | 73 |
| | 9 | 483 | 3 | 281 | 9 | 1933 | 596 | 9.7 | 20.1 | | | | | |
| Northern Ogooué tributaries | 10 | 11,135 | 1.1 | 494 | 207 | 1902 | 587 | 200 | 18 | 17.2 | 1.3 | 191.6 | 14.8 | 94 |
| | 11 | 2049 | 0.8 | 590 | 39 | 1935 | 597 | 27.2 | 13.3 | 13.2 | 1.0 | 27.1 | 2.0 | 122 |
| | 12 | 8803 | 0.5 | 523 | 169 | 1967 | 607 | 174.5 | 19.8 | 13.9 | 1.0 | 122.2 | 8.9 | 117 |
| | 13 | 49,503 | 0.6 | 549 | 949 | 1960 | 604 | 560.9 | 11.3 | 8.3 | 0.6 | 409.4 | 29.1 | 196 |
| | 19 | 1161 | 1.5 | 592 | 29 | 2579 | 795 | 52.7 | 45.4 | 48.9 | 3.7 | 56.7 | 4.3 | 33 |
| Southern Ogooué tributaries | 21 | 7582 | 1.6 | 531 | 176 | 2368 | 730 | 399.6 | 52.7 | 50.8 | 3.9 | 385.5 | 29.7 | 32 |
| | 22 | 2020 | 1.3 | 394 | 44 | 2236 | 690 | 100 | 49.5 | 29.7 | 2.3 | 60.0 | 4.6 | 55 |
| | 23 & 24 | 7057 | 1.8 | 493 | 145 | 2103 | 649 | 240.2 | 34 | 37.4 | 2.9 | 263.7 | 20.7 | 43 |
| | 25 | 379 | 2 | 322 | 7 | 1890 | 583 | 11.9 | 31.4 | 21.3 | 1.7 | 8.1 | 0.6 | 76 |
| | 14 | 4513 | 0.8 | 458 | 101 | 2287 | 705 | 54.6 | 12.1 | 36.3 | 2.9 | 163.7 | 13.0 | 45 |
| Batéké Plateaux | 15 | 4911 | 1.4 | 537 | 129 | 2692 | 830 | 42.8 | 8.7 | 18.5 | 1.4 | 91.0 | 6.6 | 87 |
| | 16 | 5892 | 1.6 | 524 | 155 | 2682 | 827 | 48 | 8.2 | 58.9 | 4.7 | 346.8 | 27.5 | 28 |
| Ogooué catchment average | at Lambaréné | 205,585 | 1.2 | 467 | 4341* | 2159 | 666 | 4071 | 19.8 | 39.3 | 3.1 | 8077.5 | 632.9 | 41 |
| Northern Ogooué tributaries | sum/ average | 80,238 | 0.8 | 528 | 1528 | 1947 | 3581 | 1150 | 14.3 | 11.7 | 0.9 | 934.9 | 69.0 | 133 |
| Southern Ogooué tributaries | sum/ average | 18,199 | 1.6 | 501 | 401 | 2254 | 678 | 804 | 44.2 | 42.5 | 3.3 | 774.0 | 59.9 | 37 |
| Batéké Plateaux | sum/ average | 15,317 | 1.3 | 509 | 385 | 2569 | 792 | 145 | 9.5 | 39.3 | 3.1 | 601.6 | 47.2 | 40 |
| | sum/ average | 46,558 | | | | | 721 | 907 | 11.5 | 62.5 | 17.4 | 5767.0 | 808.9 | |
| Mbei tributaries | sum/ average | 166 | 1.7 | 614 | 3.3 | 2011 | 620 | 2.4 | 14.5 | 21.9 | 9.2 | 3.6 | 0.3 | 71 |
| | 20n | 14,402 | 1.0 | 404 | | 2280 | | 230.9 | 16.0 | 83.4 | 16.5 | 1201.3 | 237.9 | |
| | 26n | 21,206 | 0.7 | 409 | | 2063 | | 571.9 | 27.0 | 159.7 | 36.8 | 3386.9 | 779.6 | |
| Nested | 8n | 6804 | 2.9 | 397 | | 1920 | | 43 | 6.3 | −73.0 | 154.8 | −496.7 | 1053.3 | |
| | 5n | 37,008 | 2.0 | 341 | | 2231 | | 886.2 | 23.9 | 38.4 | 31.5 | 1419.8 | 1164.8 | |
| | 10n | 9086 | 1.2 | 472 | | 1895 | | 172.8 | 19.0 | 18.1 | 1.8 | 164.5 | 16.8 | |

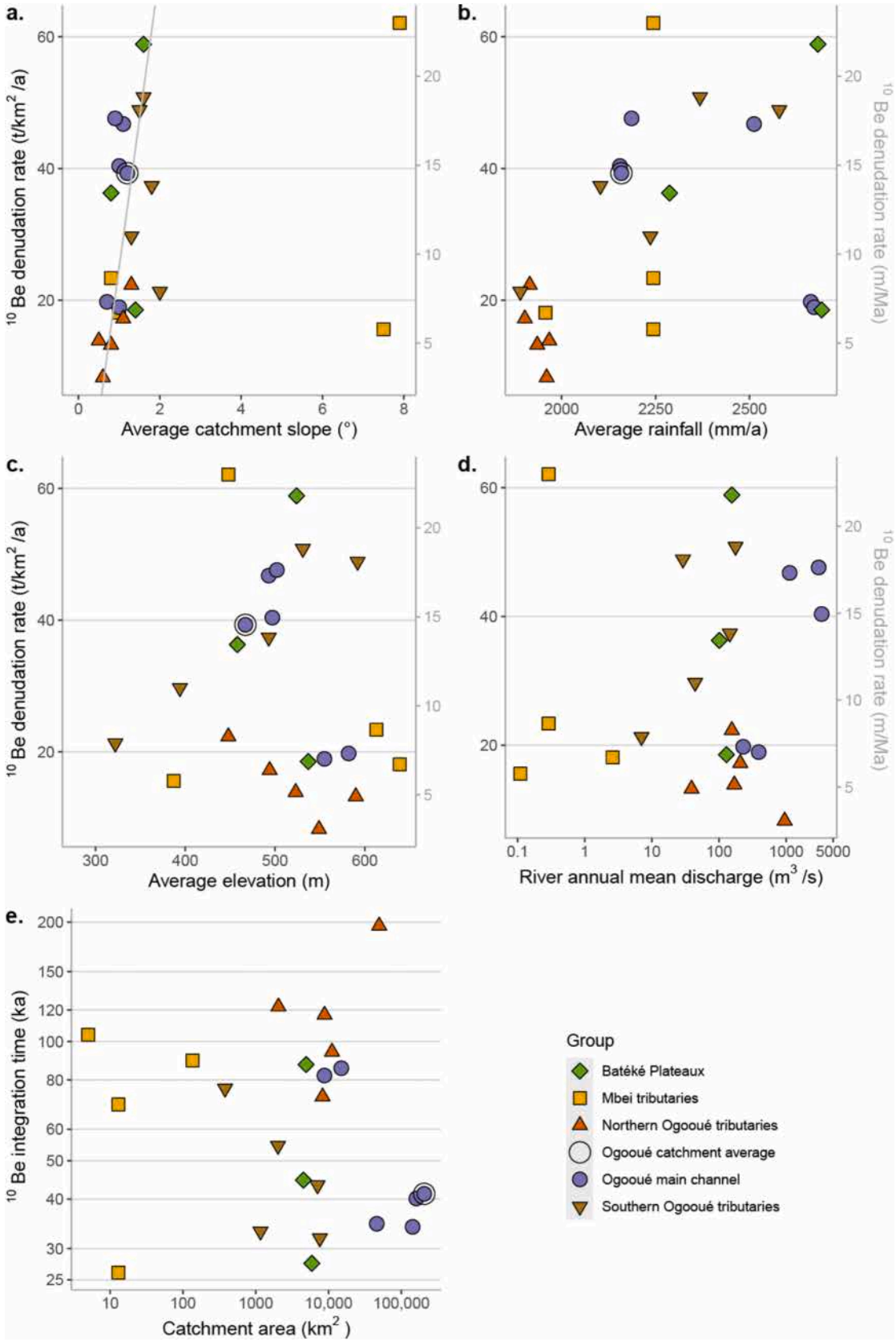


**Fig. 7.** a. Catchment-scale $^{10}$Be denudation rate vs. catchment average slope. b. Catchment-scale $^{10}$Be denudation rate vs. catchment average rainfall. c. Catchment-scale $^{10}$Be denudation rate vs. catchment average elevation, d. Catchment-scale $^{10}$Be denudation rate vs. river discharge. e. $^{10}$Be integration time vs. catchment area (in log scale). Note that the integration times are, by definition, inversely proportional to the $^{10}$Be denudation rates.

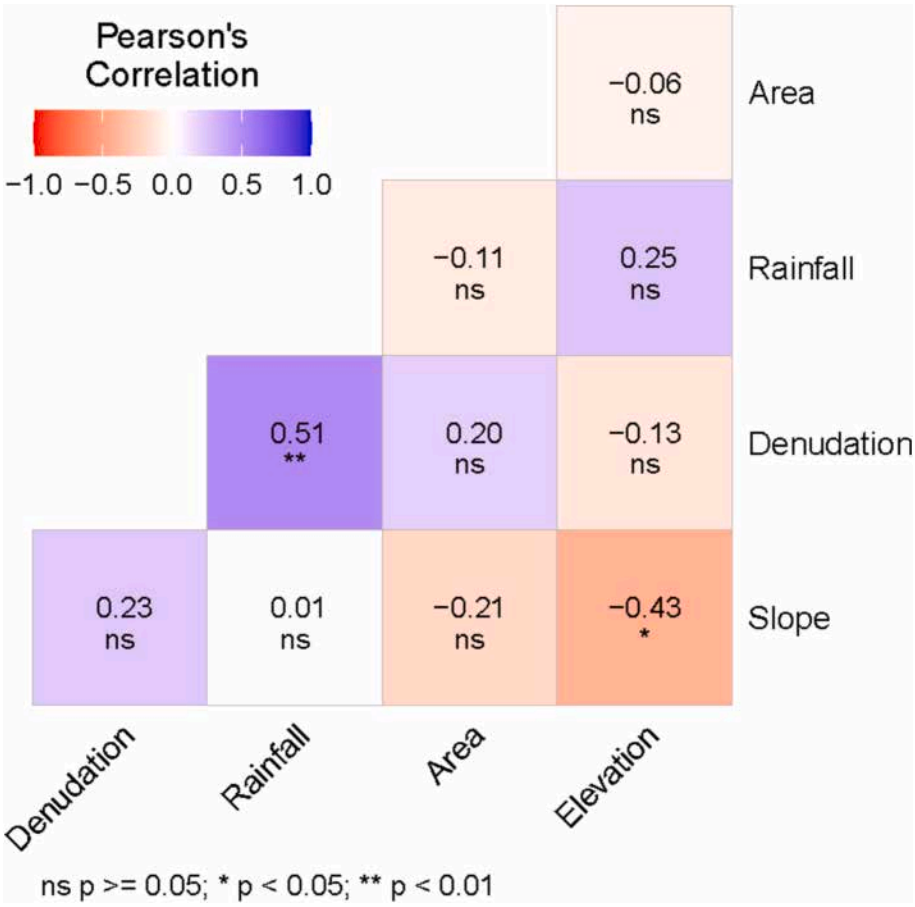


**Fig. 8.** Pearson correlation matrix between the catchment-scale $^{10}$Be denudation rate ("Denudation"), catchment area, catchment average rainfall, catchment average slope and catchment average denudation. "ns": not significant; we note that most of the correlations are not significant.

tributaries. Conversely, the denudation rates increase with the size of the catchment, except for the northern tributaries.

### 4.2. *$^{10}$Be millennial denudation rates vs. Modern denudation*

Fig. 9 represents our millennial cosmogenic $^{10}$Be flux *vs.* the modern TDS specific flux (Table 4). It is important to note that these two methods differ both in terms of the types of processes they account for (physical + part of chemical for $^{10}$Be *vs.* chemical for solute fluxes) and the time scale over which they integrate these processes (millennial for $^{10}$Be *vs.* several years for solute fluxes). Assuming that the determined modern chemical denudation rates have prevailed over the last two hundred thousand years (maximum $^{10}$Be integration time), the 1:1 line drawn in Fig. 9 corresponds to sites where denudation is only chemical (congruent dissolution, no transport), whereas the 2:1 line delineates the case of equal contributions from chemical and physical denudation. However, in this tropical cratonic type of environment, the regolith is often thick (≫ 1 m), and the $^{10}$Be measurements do not record the chemical denudation that is mostly taking place at the weathering front, i.e. at the base of the regolith. Thus, in the ORB, $^{10}$Be probably only reflects physical erosion and therefore the 1:1 line would represent locations with equal rates of chemical and physical denudation and the 2:1 line would indicate locations where chemical denudation accounts for $^{1}/_{3}$ of the total denudation ($^{2}/_{3}$ of the physical denudation). As congruent rock dissolution is rare (since it would require releasing elements that are insoluble such Al and Fe into a solution), data points lying on or below the 1:1 line can only be explained if the $^{10}$Be measurement cannot record anything about the weathering, as it occurs too deeply below the $^{10}$Be production zone and/or chemical weathering has recently increased and/or analytical issues have arisen.

In addition, in Fig. 9, the points may be shifted either to the right in the areas that underwent a recent increase in the chemical denudation rates (area below the 1:1 line) or to the left in areas that underwent a recent decrease (area above the 2:1 line). This is the case for the southern Ogooué tributaries, as two of them display points below the 1:1 line (sample points OG-22 and OG-25; the latter corresponds to the smallest documented catchment excluding the Mbei tributaries).

In Fig. 9, data from the southern and northern tributaries of the Ogooué as well as from the Mbei tributaries, plot close to the 1:1 line, suggesting that chemical denudation represents a significant part of the total denudation in these regions (i.e. the chemical denudation is of the same order of magnitude as the physical erosion). Conversely, the Batéké Plateaux area is characterized by a lower contribution of chemical weathering processes to the total denudation.

## 5. Discussion

### 5.1. *Distribution of denudation rates within the Ogooué catchment*

Our data confirm that the Ogooué catchment can be subdivided into distinct sub-areas (Figs. 4 to 7). In particular, most sub-catchments show that chemical denudation significantly contributes ($> {}^{1}/_{3}$) to the total denudation, as observed in many similar cratonic areas (Fig. 9). An exception to this general behavior includes the river draining the Batéké Plateaux and one Mbei tributary (OG-01). The Batéké Plateaux are characterised by high physical erosion rates and low chemical denudation rates (Fig. 9). The northern Ogooué catchments are characterized by: 1) a decrease in the denudation rate with catchment area (Fig. 7e), 2)

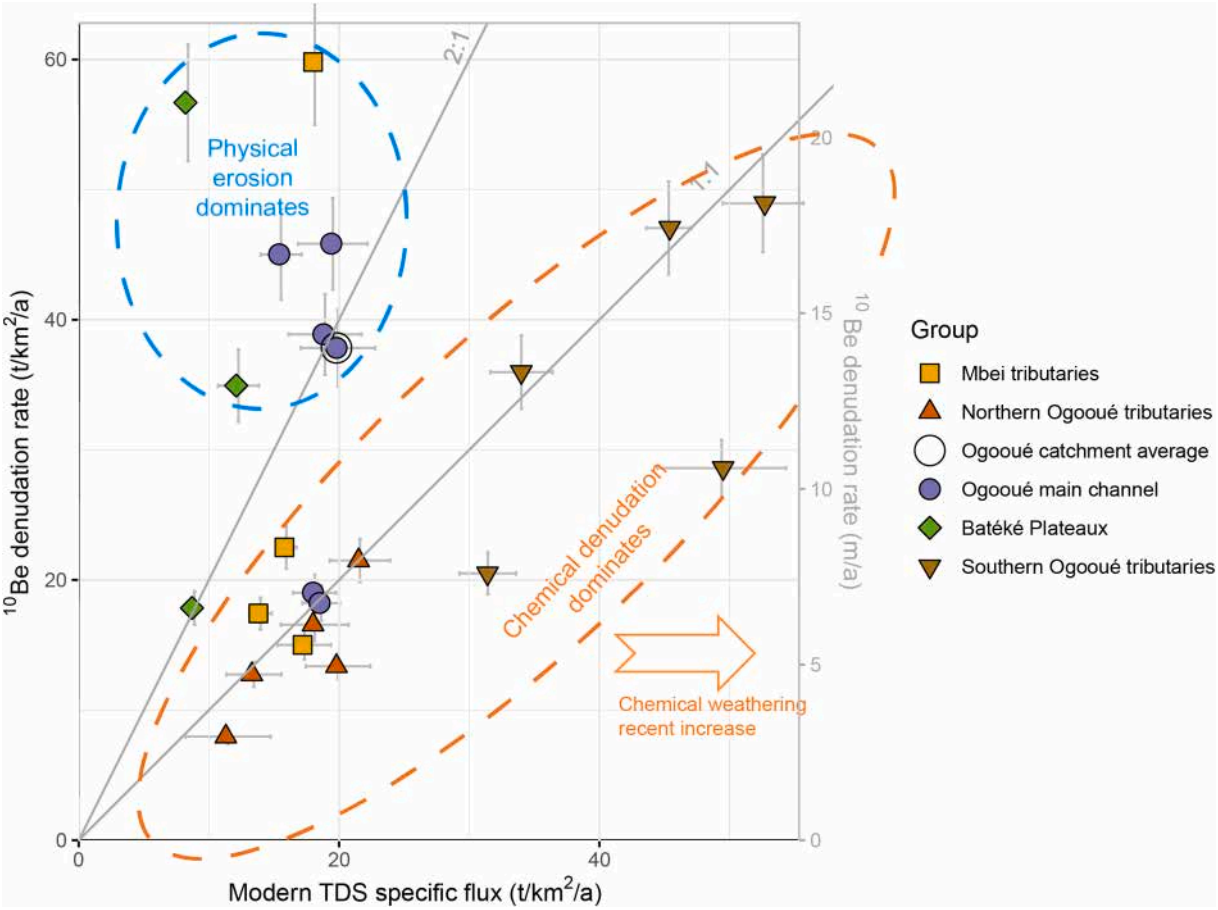


**Fig. 9.** Millennial $^{10}$Be denudation rate *vs* modern TDS specific flux (from Moquet et al. 2021). Horizontal and vertical bars indicate uncertainties. The orange ellipse delineates a group of points lying close to the 1:1 line, corresponding to catchments where chemical denudation is dominant. The blue ellipse indicates catchments where denudation occurs mainly as physical denudation while the orange ellipse indicates catchments where denudation occurs mainly as chemical weathering. Given that the two approaches yield fluxes averaged over different characteristic times, a recent increase in chemical denudation should shift the points to the right, indicated by the arrow (see text). (For interpretation of the references to color in this figure legend, the reader is referred to the web version of this article.)

**Fig. 10.** View of a "cirque" in the Batéké Plateaux. This landform is similar to the lavakas in Madagascar.

slopes and denudation rates well below the ORB average (Fig. 7a), and 3) $^{10}$Be denudation rates similar to the chemical denudation rates (Fig. 9). The southern tributaries display high denudation rates along with a significant chemical contribution (Fig. 9). In the following, each of these sub-units is discussed separately.

#### 5.1.1. Batéké Plateaux

The Batéké Plateaux area in the south-eastern part of the Ogooué catchment are underlain by mostly quartzitic aeolian unconsolidated Cenozoic sands with local sandstones (Séranne et al., 2008; Thiéblemont et al., 2009a) and are characterized by relatively high denudation rates (20–60 t/km$^2$/a or 7–22 m/Ma) with a small contribution of chemical denudation (< 15 t/km$^2$/a, Fig. 9). This prominent role of physical processes in the denudation of this region reflects the combination of two characteristics: (i) the initial material (quartzitic aeolian sands) corresponds to the product of ancient alteration episodes and is no longer prone to weathering (except for the alteration of disseminated oxides, which gives the sands their pink to red color, Fig. 10); and (ii) the material is mainly unconsolidated and susceptible to mechanical erosion. This interpretation is confirmed by field observations of active erosion and incision in sandy formations with little cohesion. In particular, regressive erosion forms were observed during our field campaigns, resulting in "badland-like" morphologies, with steaphead valleys called "cirques" filled with reworked sand (Fig. 10). The escarpments delineating these valleys locally display slopes > 45° at the level of the bordering crests.

#### 5.1.2. Northern tributaries

The catchments of the northern tributaries are characterized by shallow slopes and a low denudation rate, the magnitude of which is close to chemical denudation (8–22 t/km$^2$/a; Fig. 9). The whole area forms a plateau in continuity with the south of Cameroon, where low erosion and chemical denudation rates are also observed (Regard et al., 2016). These observations could indicate either a dominance of chemical processes on the total denudation, and/or a recent increase in the chemical denudation rates. The relief of the area drained by the northern tributaries is relatively flat, with not much variation in rock type, which may explain the low denudation rates and the high contribution of the chemical denudation.

#### 5.1.3. Southern tributaries

The southern tributaries show a relatively high rate of erosion, of the same order of magnitude as the Batéké Plateaux. However, unlike in the Batéké Plateaux, erosion in the southern ORB is associated with significant chemical denudation (Fig. 9). Indeed, the basement of the southern tributaries mainly consists of granitoids (Chaillu Massif) and Francevillian sedimentary rocks (mainly sandstones and shales) prone to chemical weathering (abundant feldspars). The relief is indeed more marked than in the north (except for greenstone belts) which could favor both physical erosion and weathering (D. Thiéblemont, pers comm).

#### 5.1.4. Mbei tributaries

The Mbei tributaries correspond to small catchments outside of the Ogooué Basin but which drain similar lithologies. Two of the corresponding samples (OG-03 and OG-04) drain a plateau area with low average slopes, whereas two other samples (OG-01 and OG-02) were collected in rivers draining the edge of the Mbei catchment, which is characterized by higher slopes. Across these samples, the denudation is low (14–22 t/km$^2$/a or 5–9 m/Ma), and the ratio between the $^{10}$Be-derived erosion rates and solute-flux derived chemical denudation is between 1 and 2, with the notable exception of OG-01 (Fig. 9). Except for OG-01, these catchments behave similarly to the northern Ogooué tributaries, with either a dominance of chemical processes on total denudation, and/or a recent increase in the chemical denudation rates. However, the Mbei tributaries lie slightly closer to the 2:1 line in Fig. 9 than the other Ogooué tributaries do, perhaps reflecting the proximity of the plateau edge where a recent increase in denudation is likely.

#### 5.1.5. Ogooué mainstream

Apart from the two most upstream points where low denudation rates are recorded, no significant change in denudation is observed along the Ogooué mainstream (around 15 m/Ma or 40 t/km$^2$/a). The erosion rates estimated through the "nested catchment approach" suggest a fast denudation of the river alluvial plain (~100 t/km$^2$/a), although these estimates are associated with strong uncertainties.

#### 5.1.6. Summary of the denudation spatial distribution

To summarize, the northern Ogooué sub-catchments are eroding more slowly than the southern counterparts, including those draining the Batéké Plateaux. At first sight, this difference can be explained by the (slightly) steeper slopes in the south (Fig. 7a). These steeper slopes are not due to differences in elevation (Fig. 7c), but instead reflect a more incised topography and a more pronounced relief (see Fig. 1). Another explanation is that the higher denudation rates could reflect a transient adjustment over long timescales, as proposed by Vanacker et al. (2007) to explain the difference in Sri Lanka between low denudation rate areas for large river systems in the coastal plains (~5 m/Ma), and high denudation rates in the highlands (~45 m/Ma). This latitudinal distinction among the Ogooué sub-catchments was already noted by Moquet et al. (2021) based on the hydrochemistry and solute fluxes. Moquet et al. (2021) proposed that this difference in terms of chemical weathering rates could be caused by uplift in the southern region, potentially related to a mantle-induced dynamic uplift or lithospheric processes affecting the rims of the Congo Cuvette located to the south of the Ogooué catchment. We are therefore now able to view this latitudinal difference in terms of the total denudation rates, which are on the order of 40 t/km$^2$/a (15 m/Ma) across the southern part of the Ogooué catchment (including the Batéké Plateaux), and less than half (~15 t/km$^2$/a or 6 m/Ma) in the northern part of the study area (including the Mbei catchments).

Within this pattern, there is no influence of integration time scales which, in any case, are always longer than the age of the last glaciation, and sometimes up to almost 200 ka. As observed elsewhere (e.g. Regard et al., 2016), there does not seem to be any noticeable evolution in the processes at a time scale of the Quaternary glacial climate cycles.

### 5.2. Low denudation rates at the scale of the whole Ogooué catchment

The contribution of the Ogooué River to the total West African Equatorial (Atlantic coast from Senegal to Angola) discharge is ~ 7 % (Moquet et al., 2021) for a contributory surface area of 2.6 %. In comparison, the solute flux of the Ogooué River, 4.1 Mt/yr, is 5 % of the total solute flux of West Africa (Milliman and Farnsworth, 2011; Moquet et al., 2021). The millennial-scale denudation flux is 8.1 Mt/a (38 t/km$^2$/a), including physical erosion and part of the TDS (see section 4.3) at the West African scale, and corresponding to 4 to 6 % of the total denudation flux (TSS + TDS ~ 220 Mt/a and TSS ~ 130 Mt/a only, evaluated over the same area as in Milliman and Farnsworth, 2011). Therefore, although the Ogooué catchment is characterized by a low rate of weathering compared to the global average, this rate is higher than the West African Equatorial average (21 *vs.* 11 t/km$^2$/a). Similarly, the millennial-scale total denudation rate is low (15 m/Ma) and is characteristic of stable cratonic areas (e.g. Beauvais and Chardon, 2013; Regard et al., 2016), but is slightly higher than the corresponding West African Equatorial average (38 *vs.* 26 t/km$^2$/a).

To compare our Ogooué data with other settings worldwide, Fig. 11 shows a compilation of the $^{10}$Be-derived denudation rates measured in cratonic areas plotted against the corresponding solute fluxes representing the rate of chemical weathering. The Ogooué data are close to the 1:1 line, meaning that the chemical to total denudation ratio is high in this catchment. This prevalence of chemical processes on the total denudation is relatively rare among cratonic catchments, even when

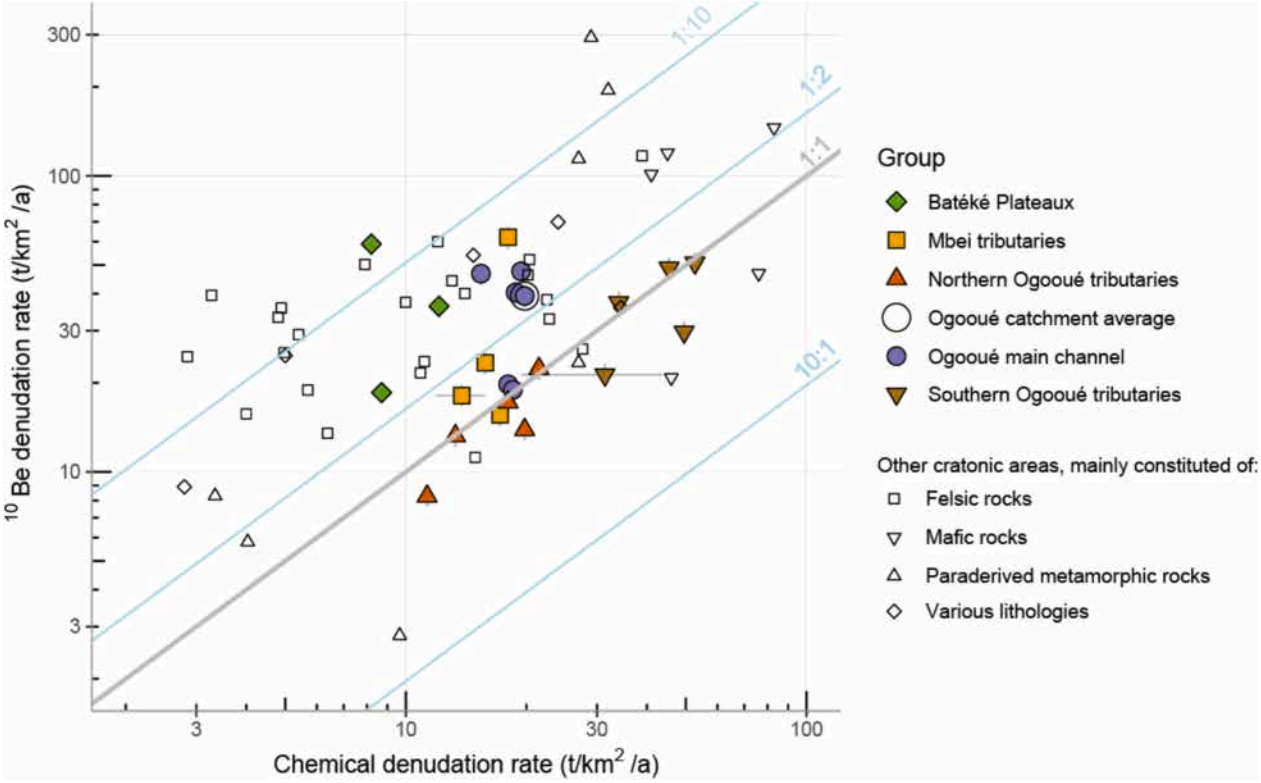


**Fig. 11.** Millennial $^{10}$Be-derived denudation rates *vs.* modern solute specific flux (in logarithmic scale) for ORB and other rivers draining cratonic areas worldwide: Oubangi, Congo, Niger, Zambesi, Fish, Molopo, Orange, Okavango, Limpopo, Murray and Darling, Finke, Macumba, Neales, St. Lawrence, Mississippi, Volga, Dniepr, Lena (Wittmann et al., 2020); Mpanga North, Dunga, Igasa, Ruimi, Mobuku, Isebo, Kilembe, Mpanga South, Dura (Hinderer et al., 2013); Maracuja, Caraca (Salgado et al., 2007); Cristiano Otoni, Sao Geraldo (Cherem et al., 2012b, 2012a); Selenga, Turka, Barguzin, Upper Angara, Kichera (Suhrhoff et al., 2022); Nyong, Mengong, Bivesse, Awout, Soo, Mbam, Sanaga (Regard et al., 2016), Branco and Tapajos (Filizola and Guyot, 2009; Wittmann et al., 2011). The lithology indicated in the legend has been evaluated from the original publications and from the GLiM databse (Hartmann and Moosdorf, 2012). The lines show the particular ratios between the chemical denudation and $^{10}$Be denudation rates; the 1:1 line depicts the equivalent denudation rates. [Printed in Black & White]. (For interpretation of the references to color in this figure legend, the reader is referred to the web version of this article.)

considering tropical catchments only (Fig. 11). Consequently, our study area stands out as a very stable cratonic setting, in which denudation is largely due to chemical weathering (see section 4.3). In particular, it is characterized by a thick regolith, which often occurs concurrently with relative equivalence between chemical weathering and physical denudation (Braun et al., 2012).

### 5.3. *Is denudation in the Ogooué landscape operating at equilibrium?*

In this work, we combine the estimates of the denudation rates based on solute fluxes and the $^{10}$Be measurements. Solute fluxes provide information on modern (i.e. typically integrated over several years) chemical denudation, whereas $^{10}$Be essentially provides information on longer-term physical denudation (25 to 200 ka, see Table 4), possibly encompassing a chemical denudation component for areas where the regolith is thin (< 1 m). This combination allows us to address the equilibrium status of the landscape of the study area. Denudation at equilibrium is achieved if the nature and thickness of the regolith do not change over time (e.g. Heimsath et al., 1997). This condition is more or less equivalent to the rate of downward progression of the weathering front being the same as the rate of lowering of the Earth's surface by denudation. A rigorous test of this hypothesis requires knowledge of the proportion of the rock material that is lost by dissolution at the weathering front versus what is lost upwards within the regolith. This apportionment is typically made accessible through the quantification of the depletion of soluble elements along weathering profiles (Dixon et al., 2009; Regard et al., 2016; Riebe et al., 2003; Riebe and Granger, 2013), a constraint that is not available at the moment. In addition, it would ideally be necessary to verify that modern physical denudation rates (obtained through sediment gauging) are comparable to those quantified over longer time scales based on $^{10}$Be concentrations.

However, in the case of the ORB and with the available data, we can assume that 1) the regolith is generally thick enough for the $^{10}$Be fluxes to only measure the physical denudation and 2) the $^{10}$Be-derived erosion rates are representative of modern physical erosion. Under such an assumption, equilibrium denudation means that points plotting along the 1:1 line in Figs. 9 and 11 describe landscapes where the physical denudation rate is equivalent to the chemical denudation rate. This condition is similar to what has been observed in two soil pits in southern Cameroon, immediately north of the study area (Braun et al., 1998; Regard et al., 2016). We conclude that the landscape is either at or close to equilibrium (note that we exclude the Batéké Plateaux region from this analysis, as the loss in solute there occurred during ancient weathering episodes – not necessarily in situ). In this case, the contrasted denudation rate between the northern and southern Ogooué tributaries suggests that weathering rates across the Ogooué catchments are "supply-limited", i.e. limited by physical erosion rates (e.g. Riebe et al., 2017).

## 6. Conclusion

The $^{10}$Be measurements provide information on the long-term denudation rate of the Ogooué River catchment. The temporal range is indicated by the integration time, ranging from 25 ka in the fastest denuding parts (e.g. OG-16) to 200 ka (OG-13). The integration time averaged over the entire catchment is 40 ka. The Ogooué River

catchment denudes at a relatively slow rate (38 t/km$^2$/a, 15 m/Ma), slightly higher than the West African average (~26 t/km$^2$/a, ~10 m/Ma, evaluated from Milliman and Farnsworth, 2011). Physical denudation and chemical weathering are of the same order of magnitude. This shows that, although low, there is substantial chemical weathering compared to physical denudation, with a contribution that is likely > 30 % of the total denudation.

However, this large-scale observation is associated with denudation rates that are spatially variable (10–60 t/km$^2$/a). This variability exhibits a fairly close balance of physical denudation/chemical weathering over the long term (close to the 1:1 line on Fig. 11). Noticeably, there is an overall strong correlation between the chemical denudation rates and physical erosion rates. This supports the scenario of supply-limited weathering, where chemical denudation contributes to a large part of the total denudation. The data points from the Batéké Plateaux are outside this trend, because they are made up of detrital material that has already been weathered and therefore they have a very low modern flux of solutes. The results of this study confirm and complement the work of Moquet et al. (2021), i.e. the southern part of the catchment is denuding twice as fast as the northern part, and that denudation over the whole catchment has not varied much since 100 ka, as shown by both methods which give consistent results. Higher denudation rates to the south could be caused by uplift (Guillocheau et al., 2018). Uplift in the area may operate over a long wavelengths (> 1000 km), spanning a time scale of millions of years, and could be due to deep-seated mantle upwelling (e.g. Cottrell et al., 2004; Guillocheau et al., 2018; Hu et al., 2018).

## Funding

This study was supported by the RALTERAC EC2CO INSU project, the International Joint Laboratory DYCOFAC (Dynamics of the forested ecosystems of Central Africa in a context of global change) and the Programme Emergences of the City of Paris “Chemical weathering of sediments in large tropical floodplains” (agreement 205DDEEES165). The $^{10}$Be and $^{26}$Al analyses were performed at the ASTER AMS national facility (CEREGE, Aix-en-Provence), and were supported by the INSU/CNRS, the ANR through the “Projets thématiques d’excellence” program for the “Equipements d’excellence” ASTER-CEREGE action, and the Institut de Recherche pour le Développement (IRD).

## CRediT authorship contribution statement

**V. Regard:** Writing – review & editing, Writing – original draft, Visualization, Validation, Methodology, Funding acquisition, Formal analysis, Conceptualization. **S. Carretier:** Writing – review & editing, Investigation. **J.-S. Moquet:** Writing – review & editing, Writing – original draft, Validation, Resources, Conceptualization. **S. Choy:** Writing – review & editing, Writing – original draft, Investigation. **P.-H. Blard:** . **S. Bogning:** Writing – review & editing, Investigation. **A.P. Mbonda:** Writing – review & editing, Investigation. **E. Mambela:** Writing – review & editing, Investigation. **M.C. Paiz:** Writing – review & editing, Investigation. **M. Séranne:** Writing – review & editing, Validation, Resources. **J. Charreau:** Writing – review & editing, Validation, Resources. **D. Rouby:** Writing – review & editing, Validation. **J. Bouchez:** Writing – review & editing, Validation, Funding, Conceptualization. **J. Gaillardet:** Writing – review & editing, Funding, Validation. **J.-J. Braun:** Writing – review & editing, Writing – original draft, Visualization, Validation, Methodology, Funding acquisition, Conceptualization. **Y. Denèle:** Writing – review & editing.

## Declaration of competing interest

The authors declare that they have no known competing financial interests or personal relationships that could have appeared to influence the work reported in this paper.

## Acknowledgements

We would especially like to thank Dr. Aurélie Flore Koumba Pambo for the research authorizations in Gabon, Jean-Grégoire Kayoum for driving and taking photographs during the sampling field campaign, and D. Thiéblemont (BRGM) for constructive discussions about the geology of the Ogooué catchment. We would also like to thank the ANPN and CIRMF for their support during the field campaign. This work is a contribution of the dating facility at GET in Toulouse. The measurements were performed at the ASTER national accelerator mass spectrometry facility (CEREGE, Aix-en- Provence) that is supported by INSU/CNRS, ANR and IRD; we warmly thank ASTER Team (Georges Aumaître, Didier Bourlès (†), Karim Keddadouche). We are very grateful for the strong support from the GET lab and from ANR PANTERA. Verle Vanacker, Denis Thiéblemont and Jan Marten Huizenga are acknowledged for their fruitful comments. We are indebted to Sara Mullin for the English editing.

### *Author contributions*

Conceptualization: JJB, JSM, VR, SCa, JB; funding acquisition: JJB, JB, VR; field work: JSM, JJB, SB, MS and APM; cosmogenic nuclide measurements and data analysis: VR, SCa, SCh, PHN, JC; writing-original draft: VR, SCa & JSM; writing-review and editing: all authors.

## References

Al-Hajri, Y., White, N., Fishwick, S., 2009. Scales of transient convective support beneath Africa. Geology 37, 883–886. https://doi.org/10.1130/G25703A.1.

Arnold, M., Merchel, S., Bourlès, D.L., Braucher, R., Benedetti, L., Finkel, R.C., Aumaître, G., Gottdang, A., Klein, M., 2010. The French accelerator mass spectrometry facility ASTER: Improved performance and developments. Nucl. Instrum. Methods Phys. Res. Sect. B Beam Interact. Mater. at., 19th International Conference on Ion Beam Analysis 268, 1954–1959. https://doi.org/10.1016/j.nimb.2010.02.107.

Balco, G., Stone, J.O., Lifton, N.A., Dunai, T.J., 2008. A complete and easily accessible means of calculating surface exposure ages or erosion rates from Be-10 and Al-26 measurements. Quat. Geochronol. 3, 174–195.

Beauvais, A., Chardon, D., 2013. Modes, tempo, and spatial variability of Cenozoic cratonic denudation: The West African example. Geochem. Geophys. Geosystems 14, 1590–1608. https://doi.org/10.1002/ggge.20093.

Bogning, S., Frappart, F., Blarel, F., Nino, F., Mahé, G., Bricquet, J.-P., Seyler, F., Onguéné, R., Etame, J., Paiz, M.-C., 2018. Monitoring water levels and discharges using radar altimetry in an ungauged river basin: The case of the Ogooué. Remote Sens. 10, 350.

Braucher, R., Merchel, S., Borgomano, J., BourlÃs, D.L., 2011. Production of cosmogenic radionuclides at great depth: A multi element approach. Earth Planet. Sci. Lett. 309, 1–9. Doi: 10.1016/j.epsl.2011.06.036.

Braucher, R., Guillou, V., Bourlès, D.L., Arnold, M., Aumaître, G., Keddadouche, K., Nottoli, E., 2015. Preparation of ASTER in-house 10Be/9Be standard solutions. Nucl. Instrum. Methods Phys. Res. Sect. B Beam Interact. Mater. At. The Thirteenth Accelerator Mass Spectrometry Conference 361, 335–340. https://doi.org/10.1016/j.nimb.2015.06.012.

Braun, J.-J., Viers, J., Dupré, B., Polve, M., Ndam, J., Muller, J.-P., 1998. Solid/Liquid REE Fractionation in the Lateritic System of Goyoum, East Cameroon: The Implication for the Present Dynamics of the Soil Covers of the Humid Tropical Regions. Geochim. Cosmochim. Acta 62, 273–299. https://doi.org/10.1016/S0016-7037(97)00344-X.

Braun, J.-J., Marechal, J.-C., Riotte, J., Boeglin, J.-L., Bedimo Bedimo, J.-P., Ndam Ngoupayou, J.R., Nyeck, B., Robain, H., Sekhar, M., Audry, S., Viers, J., 2012. Elemental weathering fluxes and saprolite production rate in a Central African lateritic terrain (Nsimi, South Cameroon). Geochim. Cosmochim. Acta 99, 243–270. https://doi.org/10.1016/j.gca.2012.09.024.

Burbank, D.W., Leland, J., Fielding, E., Anderson, R.S., Brozovic, N., Reid, M.R., Duncan, C., 1996. Bedrock incision, rock uplift and threshold hillslopes in the northwestern Himalayas. Nature 379, 505–510. https://doi.org/10.1038/379505a0.

Carré, P., 1978. Fleuves et rivières du Gabon. Diversité des régimes hydrologiques. 24 p., 2cartes. République gabonaise. Centre national de la recherche scientifique et technologique. Sectiond’études et recherches en hydrologie.

Carretier, S., Regard, V., Vassallo, R., Aguilar, G., Martinod, J., Riquelme, R., Pepin, E., Charrier, R., Hérail, G., Farías, M., Guyot, J.-L., Vargas, G., Lagane, C., 2013. Slope and climate variability control of erosion in the Andes of central Chile. Geology 41, 195–198. https://doi.org/10.1130/G33735.1.

Carretier, S., Regard, V., Vassallo, R., Martinod, J., Christophoul, F., Gayer, E., Audin, L., Lagane, C., 2015. A note on $^{10}$Be-derived mean erosion rates in catchments with heterogeneous lithology: examples from the western Central Andes. Earth Surf. Process. Landf. 40, 1719–1729. https://doi.org/10.1002/esp.3748.

Charreau, J., Blard, P.-H., Zumaque, J., Martin, L.C.P., Delobel, T., Szafran, L., 2019. Basinga: A cell-by-cell GIS toolbox for computing basin average scaling factors, cosmogenic production rates and denudation rates. Earth Surf. Process. Landf. 44, 2349–2365. https://doi.org/10.1002/esp.4649.

Cherem, L.F.S., Varajão, C.A.C., Braucher, R., Bourlés, D., Salgado, A.A.R., Varajão, A.C., 2012a. Long-term evolution of denudational escarpments in southeastern Brazil. Geomorphology 173–174, 118–127. https://doi.org/10.1016/j.geomorph.2012.06.002.

Cherem, L.F.S., Varajão, C.A.C., Salgado, A.A.R., Varajão, A.F.D.C., Braucher, R., Bourlés, D., Júnior, A.P.M., Júnior, H.Á.N., 2012b. DENUDAÇÃO QUÍMICA E REBAIXAMENTO DO RELEVO EM BORDAS INTERPLANÁLTICAS COM SUBSTRATO GRANÍTICO: DOIS EXEMPLOS NO SE DE MINAS GERAIS. Rev. Bras. Geomorfol. 13. https://doi.org/10.20502/rbg.v13i1.344.

Chmeleff, J., von Blanckenburg, F., Kossert, K., Jakob, D., 2010. Determination of the Be-10 half-life by multicollector ICP-MS and liquid scintillation counting. Nucl. Instrum. Methods Phys. Res. Sect. B-Beam Interact. Mater. at. 268, 192–199.

Codilean, A.T., Munack, H., Cohen, T.J., Saktura, W.M., Gray, A., Mudd, S.M., 2018. OCTOPUS: an open cosmogenic isotope and luminescence database. Earth Syst. Sci. Data 10, 2123–2139. https://doi.org/10.5194/essd-10-2123-2018.

Cottrell, E., Jaupart, C., Molnar, P., 2004. Marginal stability of thick continental lithosphere. Geophys. Res. Lett. 31. https://doi.org/10.1029/2004GL020332.

DiBiase, R.A., 2018. Short communication: Increasing vertical attenuation length of cosmogenic nuclide production on steep slopes negates topographic shielding corrections for catchment erosion rates. Earth Surf. Dyn. 6, 923–931. https://doi.org/10.5194/esurf-6-923-2018.

Dixon, J.L., Heimsath, A.M., Amundson, R., 2009. The critical role of climate and saprolite weathering in landscape evolution. Earth Surf. Process. Landf. 34, 1507–1521. https://doi.org/10.1002/esp.1836.

Ferrier, K.L., Kirchner, J.W., 2008. Effects of physical erosion on chemical denudation rates: A numerical modeling study of soil-mantled hillslopes. Earth Planet. Sci. Lett. 272, 591–599. https://doi.org/10.1016/j.epsl.2008.05.024.

Filizola, N., Guyot, J.L., 2009. Suspended sediment yields in the Amazon basin: an assessment using the Brazilian national data set. Hydrol. Process. 23, 3207–3215. https://doi.org/10.1002/hyp.7394.

Galy, A., France-Lanord, C., 2001. Higher erosion rates in the Himalaya: Geochemical constraints on riverine fluxes. Geology 29, 23–26. https://doi.org/10.1130/0091-7613(2001)029<0023:HERITH>2.0.CO;2.

Godard, V., Bourles, D.L., Spinabella, F., Burbank, D.W., Bookhagen, B., Fisher, G.B., Moulin, A., Leanni, L., 2014. Dominance of tectonics over climate in Himalayan denudation. Geology 42, 243–246. https://doi.org/10.1130/G35342.1.

Granger, D.E., Riebe, C.S., 2007. Cosmogenic Nuclides in Weathering and Erosion. In: Drever, J.I. (Ed.), Treatise on Geochemistry, Volume 5: Surface and Ground Water, Weathering, and Soils. Elsevier, London.

Guillocheau, F., Chelalou, R., Linol, B., Dauteuil, O., Robin, C., Mvondo, F., Callet, Y., Colin, J.-P., 2015. Cenozoic Landscape Evolution in and Around the Congo Basin: Constraints from Sediments and Planation Surfaces, in: Geology and Resource Potential of the Congo Basin (de Wit, M., Guillocheau, F., de WIt M.C.J., Regional Geology Reviews. Springer, pp. 271–313.

Guillocheau, F., Simon, B., Baby, G., Bessin, P., Robin, C., Dauteuil, O., 2018. Planation surfaces as a record of mantle dynamics: The case example of Africa. Gondwana Res. Rifting to Passive Margins 53, 82–98. https://doi.org/10.1016/j.gr.2017.05.015.

Hartmann, J., Moosdorf, N., 2012. The new global lithological map database GLiM: A representation of rock properties at the Earth surface. Geochem. Geophys. Geosystems 13. https://doi.org/10.1029/2012GC004370.

Heimsath, A.M., Dietrich, W.E., Nishiizumi, K., Finkel, R.C., 1997. The soil production function and landscape equilibrium. Nature 388, 358–361. https://doi.org/10.1038/41056.

Hewawasam, T., von Blanckenburg, F., Bouchez, J., Dixon, J.L., Schuessler, J.A., Maekeler, R., 2013. Slow advance of the weathering front during deep, supply-limited saprolite formation in the tropical Highlands of Sri Lanka. Geochim. Cosmochim. Acta 118, 202–230. https://doi.org/10.1016/j.gca.2013.05.006.

Hinderer, M., Pflanz, D., Schneider, S., 2013. Chemical Denudation Rates in the Humid Tropics of East Africa and Comparison with 10Be-Derived Erosion Rates. In: Procedia Earth Planet. Sci., Proceedings of the Fourteenth International Symposium on Water-Rock Interaction. https://doi.org/10.1016/j.proeps.2013.03.047.

Hu, J., Liu, L., Faccenda, M., Zhou, Q., Fischer, K.M., Marshak, S., Lundstrom, C., 2018. Modification of the Western Gondwana craton by plume–lithosphere interaction. Nat. Geosci. 11, 203–210. https://doi.org/10.1038/s41561-018-0064-1.

Kittel, C.M., Nielsen, K., Tøttrup, C., Bauer-Gottwein, P., 2018. Informing a hydrological model of the Ogooué with multi-mission remote sensing data. Hydrol. Earth Syst. Sci. 22, 1453–1472.

Korschinek, G., Bergmaier, A., Faestermann, T., Gerstmann, U.C., Knie, K., Rugel, G., Wallner, A., Dillmann, I., Dollinger, G., von Gostomski, C.L., 2010. A new value for the half-life of 10Be by Heavy-Ion Elastic Recoil Detection and liquid scintillation counting. Nucl. Instrum. Methods Phys. Res. Sect. B Beam Interact. Mater. at. 268, 187–191. https://doi.org/10.1016/j.nimb.2009.09.020.

Kottek, M., Grieser, J., Beck, C., Rudolf, B., Rubel, F., 2006. World Map of the Köppen-Geiger climate classification updated. Meteorol. z. 15, 259–263. https://doi.org/10.1127/0941-2948/2006/0130.

Laraque, A., Bernal, C., Bourrel, L., Darrozes, J., Christophoul, F., Armijos, E., Fraizy, P., Pombosa, R., Guyot, J.L., 2009. Sediment budget of the Napo River, Amazon basin, Ecuador and Peru. Hydrol. Process. 23, 3509–3524.

Larsen, I.J., Montgomery, D.R., Greenberg, H.M., 2014. The contribution of mountains to global denudation. Geology 42, 527–530. https://doi.org/10.1130/G35136.1.

Lupker, M., Blard, P.-H., Lavé, J., France-Lanord, C., Leanni, L., Puchol, N., Charreau, J., Bourlès, D., 2012. 10Be-derived Himalayan denudation rates and sediment budgets in the Ganga basin. Earth Planet. Sci. Lett. 333–334, 146–156. https://doi.org/10.1016/j.epsl.2012.04.020.

Maffre, P., Ladant, J.-B., Moquet, J.-S., Carretier, S., Labat, D., Goddéris, Y., 2018. Mountain ranges, climate and weathering. Do orogens strengthen or weaken the silicate weathering carbon sink? Earth Planet. Sci. Lett. 493, 174–185. https://doi.org/10.1016/j.epsl.2018.04.034.

Martin, L.C.P., Blard, P.-H., Balco, G., Lavé, J., Delunel, R., Lifton, N., Laurent, V., 2017. The CREp program and the ICE-D production rate calibration database: A fully parameterizable and updated online tool to compute cosmic-ray exposure ages. Quat. Geochronol. 38, 25–49. https://doi.org/10.1016/j.quageo.2016.11.006.

Milliman, J., Farnsworth, K., 2011. River Discharge to the Coastal Ocean: A Global Synthesis. Cambridge University Press, Cambridge. https://doi.org/10.1017/CBO9780511781247.

Moquet, J.-S., Bouchez, J., Braun, J.-J., Bogning, S., Mbonda, A.P., Carretier, S., Regard, V., Bricquet, J.-P., Paiz, M.-C., Mambela, E., Gaillardet, J., 2021. Contrasted Chemical Weathering Rates in Cratonic Basins: The Ogooué and Mbei Rivers. Western Central Africa. Front. Water 2. https://doi.org/10.3389/frwa.2020.589070.

Nishiizumi, K., Imamura, M., Caffee, M.W., Southon, J.R., Finkel, R.C., McAninch, J., 2007. Absolute calibration of Be-10 AMS standards. Nucl. Instrum. Methods Phys. Res. Sect. B-Beam Interact. Mater. at. 258, 403–413.

Picouet, C., Dupré, B., Orange, D., Valladon, M., 2002. Major and trace element geochemistry in the upper Niger river (Mali): physical and chemical weathering rates and CO2 consumption. Chem. Geol. 185, 93–124. https://doi.org/10.1016/S0009-2541(01)00398-9.

Puchol, N., Charreau, J., Blard, P.-H., Lavé, J., Dominguez, S., Pik, R., Saint-Carlier, D., Team, A., 2017. Limited impact of Quaternary glaciations on denudation rates in Central Asia. Bulletin 129, 479–499.

Regard, V., Carretier, S., Boeglin, J.-L., Ndam Ngoupayou, J.-R., Dzana, J.-G., Bedimo Bedimo, J.-P., Riotte, J., Braun, J.-J., 2016. Denudation rates on cratonic landscapes: comparison between suspended and dissolved fluxes, and 10Be analysis in the Nyong and Sanaga River basins, south Cameroon. Earth Surf. Process. Landf. 41, 1671–1683. https://doi.org/10.1002/esp.3939.

Riebe, C.S., Granger, D.E., 2013. Quantifying effects of deep and near-surface chemical erosion on cosmogenic nuclides in soils, saprolite, and sediment. Earth Surf. Process. Landf. 38, 523–533. https://doi.org/10.1002/esp.3339.

Riebe, C.S., Kirchner, J.W., Finkel, R.C., 2003. Long-term rates of chemical weathering and physical erosion from cosmogenic nuclides and geochemical mass balance. Geochim. Cosmochim. Acta 67, 4411–4427. https://doi.org/10.1016/S0016-7037(03)00382-X.

Riebe, C.S., Hahm, W.J., Brantley, S.L., 2017. Controls on deep critical zone architecture: a historical review and four testable hypotheses. Earth Surf. Process. Landf. 42, 128–156. https://doi.org/10.1002/esp.4052.

Salgado, A., Varajão, C., Colin, F., Braucher, R., Varajão, A., Nalini Jr, H., 2007. Study of the erosion rates in the upper Maracujá Basin (Quadrilátero Ferrífero/MG, Brazil) by the in situ produced cosmogenic10Be method. Earth Surf. Process. Landf. 32, 905–911. https://doi.org/10.1002/esp.1448.

Scherler, D., DiBiase, R.A., Fisher, G.B., Avouac, J.-P., 2017. Testing monsoonal controls on bedrock river incision in the Himalaya and Eastern Tibet with a stochastic-threshold stream power model. J. Geophys. Res. Earth Surf. 122, 1389–1429. https://doi.org/10.1002/2016JF004011.

Şengör, A.M.C., Lom, N., Polat, A., 2022. The nature and origin of cratons constrained by their surface geology. GSA Bull. 134, 1485–1505. https://doi.org/10.1130/B36079.1.

Séranne, M., Bruguier, O., Moussavou, M., 2008. U-Pb single zircon grain dating of Present fluvial and Cenozoic aeolian sediments from Gabon: consequences on sediment provenance, reworking, and erosion processes on the equatorial West African margin. Bull. Société Géologique Fr. 179, 29–40.

Stone, J.O., 2000. Air pressure and cosmogenic isotope production. J Geophys Res 105, 23753–23759.

Suhrhoff, T.J., Rickli, J., Christl, M., Vologina, E.G., Pham, V., Belhadj, M., Sklyarov, E. V., Jeandel, C., Vance, D., 2022. Source to sink analysis of weathering fluxes in Lake Baikal and its watershed based on riverine fluxes, elemental lake budgets, REE patterns, and radiogenic (Nd, Sr) and 10Be/9Be isotopes. Geochim. Cosmochim. Acta 321, 133–154. https://doi.org/10.1016/j.gca.2022.01.007.

Thiéblemont, D., Castaing, C., Billa, M., Bouton, P., Préat, A., 2009a. Notice explicative de la carte géologique et des ressources minérales de la République Gabonaise à 1/1000000. Programme Sysmin 8, 384.

Thiéblemont, D., Castaing, C., Bouton, P., Billa, M., Prian, J.P., Goujou, J.C., Boulingui, B., Ekogha, H., Kassadou, A., Simo Ndounze, S., Ebang Obiang, M., Nagel, J.L., Abouma Simba, S., Husson, Y., 2009b. Carte géologique et des Ressources minérales de la République Gabonaise à 1/1 000 000.

Uppala, S.M., KÅllberg, P.W., Simmons, A.J., Andrae, U., Bechtold, V.D.C., Fiorino, M., Gibson, J.K., Haseler, J., Hernandez, A., Kelly, G.A., Li, X., Onogi, K., Saarinen, S., Sokka, N., Allan, R.P., Andersson, E., Arpe, K., Balmaseda, M.A., Beljaars, A.C.M., Berg, L.V.D., Bidlot, J., Bormann, N., Caires, S., Chevallier, F., Dethof, A., Dragosavac, M., Fisher, M., Fuentes, M., Hagemann, S., Hólm, E., Hoskins, B.J., Isaksen, L., Janssen, P. a. E.M., Jenne, R., Mcnally, A.P., Mahfouf, J.-F., Morcrette, J.-J., Rayner, N.A., Saunders, R.W., Simon, P., Sterl, A., Trenberth, K.E., Untch, A., Vasiljevic, D., Viterbo, P., Woollen, J., 2005. The ERA-40 re-analysis. Q. J. R. Meteorol. Soc. 131, 2961–3012. Doi: 10.1256/qj.04.176.

Vanacker, V., von Blanckenburg, F., Hewawasam, T., Kubik, P.W., 2007. Constraining landscape development of the Sri Lankan escarpment with cosmogenic nuclides in river sediment. Earth Planet. Sci. Lett. 253, 402–414. https://doi.org/10.1016/j.epsl.2006.11.003.

Viers, J., Dupré, B., Braun, J.-J., Deberdt, S., Angeletti, B., Ngoupayou, J.N., Michard, A., 2000. Major and trace element abundances, and strontium isotopes in the Nyong

basin rivers (Cameroon): constraints on chemical weathering processes and elements transport mechanisms in humid tropical environments. Chem. Geol. 169, 211–241. https://doi.org/10.1016/S0009-2541(00)00298-9.

Weber, F., Gauthier-Lafaye, F., Whitechurch, H., Ulrich, M., El Albani, A., 2016. The 2-Ga Eburnean Orogeny in Gabon and the opening of the Francevillian intracratonic basins: A review. Comptes Rendus Geosci. 348, 572–586. https://doi.org/10.1016/j.crte.2016.07.003.

Willenbring, J.K., Codilean, A.T., McElroy, B., 2013. Earth is (mostly) flat: Apportionment of the flux of continental sediment over millennial time scales. Geology G33918, 1. https://doi.org/10.1130/G33918.1.

Wittmann, H., von Blanckenburg, F., Maurice, L., Guyot, J.-L., Filizola, N., Kubik, P.W., 2011. Sediment production and delivery in the Amazon River basin quantified by in situ–produced cosmogenic nuclides and recent river loads. GSA Bull. 123, 934–950. https://doi.org/10.1130/B30317.1.

Wittmann, H., Oelze, M., Gaillardet, J., Garzanti, E., Von Blanckenburg, F., 2020. A global rate of denudation from cosmogenic nuclides in the Earth's largest rivers. Earth-Sci. Rev. 204, 103147. https://doi.org/10.1016/j.earscirev.2020.103147.

Gondwana Research 140 (2025) 158–158

Contents lists available at ScienceDirect

Gondwana Research

journal homepage: www.elsevier.com/locate/gr

Corrigendum

# Corrigendum to "Contrasting physical erosion rates in cratonic catchments: The Ogooué and Mbei rivers, Western Central Africa" [Gondwana Res. 138 (2025) 192–209]

V. Regard [a,*], S. Carretier [a], J.-S. Moquet [b], S. Choy [a], P.-H. Blard [c,d], S. Bogning [e], A.P. Mbonda [f], E. Mambela [g], M.C. Paiz [g], M. Séranne [h], J. Charreau [c], D. Rouby [a], J. Bouchez [i], J. Gaillardet [i], J.-J. Braun [a,j,k], Y. Denèle [a]

[a] GET (Université de Toulouse, CNRS, IRD, UPS, CNES), Toulouse, France
[b] Univ. Orléans, CNRS, BRGM, ISTO, UMR 7327, F-45071, Orléans, France
[c] CRPG, CNRS, Université de Lorraine, Nancy, France
[d] Laboratoire de Glaciologie, ULB, Brussels, Belgium
[e] Université de Douala, Cameroon
[f] Centre National de la Recherche Scientifique, Libreville, Gabon
[g] The Nature Conservancy, Libreville, Gabon
[h] Géosciences Montpellier, Université de Montpellier, CNRS, Montpellier, France
[i] IPGP (Université Paris Cité, CNRS, Université La Réunion, IGN), Paris, France
[j] LMI DYCOFAC IRD-University of Yaoundé 1-IRGM, BP 1857, Cameroon
[k] Agence Nationale des Parcs Nationaux, Libreville, Gabon

The authors regret that the additional material on the paper was lost during the final improvement of the article.

The authors would like to apologise for any inconvenience caused.

## Appendix A. Supplementary material

Supplementary data to this article can be found online at https://doi.org/10.1016/j.gr.2024.12.004.

DOI of original article: https://doi.org/10.1016/j.gr.2024.10.013.
* Corresponding author at: 14 av. Edouard Belin, 31400 Toulouse, France.
*E-mail address:* Vincent.regard@get.omp.eu (V. Regard).

https://doi.org/10.1016/j.gr.2024.12.004

Available online 20 December 2024